2014

TUMOR-PENETRATING ACETALATED DEXTRAN NANOPARTICLES CAPABLE OF TANDEM DELIVERY OF AGENTS FOR THE TREATMENT OF LUNG CANCER

Qihua Sun
University of Rhode Island, qihuasun900514@gmail.com

TUMOR-PENETRATING ACETALATED DEXTRAN NANOPARTICLES CAPABLE OF TANDEM DELIVERY OF AGENTS FOR THE TREATMENT OF LUNG CANCER

BY

QIHUA SUN

A THESIS SUBMITTED IN PARTIAL FULFILLMENT OF THE

REQUIREMENTS FOR THE DEGREE OF

MASTER OF SCIENCE

IN

CHEMICAL ENGINEERING

UNIVERSITY OF RHODE ISLAND

2014

MASTER OF SCIENCE THESIS

OF

QIHUA

APPROVED:

Thesis Committee:

Major Professor Samantha Meenach

Geoffrey D. Bothun

Wei Lu

Nasser H. Zawia
DEAN OF THE GRADUATE SCHOOL

UNIVERSITY OF RHODE ISLAND

2014

ABSTRACT

The overall survival rate for patients diagnosed with lung cancer is still extremely low and many affected patients are not eligible for first-line treatments such as surgery, chemotherapy, and radiation for the treatment due to the severe side effects associated with these therapies. Paclitaxel (PTX) along with imatinib mesylate are currently first-line therapies for many types of cancer (Kelly 2001, Schiller 2002). However, the successful delivery of paclitaxel faces many challenges due to its lipophilic nature and high protein affinity, which often results in low bioavailability. Solubilization of drugs such as PTX, enhanced tumor accumulation, and toxicity attenuation of such therapeutics can be enhanced via targeted delivery to tumors using nanoparticles (NPs). For example, chemotherapeutic drugs such as PTX and doxorubicin have been encapsulated singularly in micelles (Jinhyang 2012) and nanoliposomes (Zhang 2011), thereby increasing the efficacy of radiation therapy against *in vitro* lung cancer cells and in animals, demonstrating the success of nanoparticle-mediated treatment of cancer. Current cancer treatment, however, revolves around the tandem delivery of PTX and therapeutics such as imatinib, doxorubicin, and carboplatin. Unfortunately, multi-drug delivery is not easily achieved with single-agent delivery systems demonstrating the need for a nanoparticle system capable of delivering multiple drugs in tandem directly to the tumor site(s).

While the enhanced permeability and retention (EPR) effect has served as a key rationale for using nanoparticles to treat solid tumors, as it allows for increased uptake of NPs at the tumor site, it often does not enable uniform delivery of these particles to all regions of tumors. Tumor-penetrating peptides show great promise in overcoming

the relevant physiological barriers preventing accumulation and penetrating into the avascular region of tumors. iRGD (internalizing RGD, CRGDKDPDC), has been shown to effectively target and penetrate both *in vitro* multicellular spheroids (MCS) and *in vivo* animal model tumors when conjugated to drugs or nanoparticles (Sugahara 2010). For the described research, I hypothesize that iRGD-conjugated nanoparticles containing PTX and imatinib will more effectively home to and penetrate lung cancer tumor spheroids for more effective treatment of this dismal disease.

In particular, acetalated dextran (Ac-Dex) nanoparticles were synthesized to contain PTX and/or imatinib. These particles were shown to have sizes appropriate for systemic delivery (approximately 250 nm) and exhibited smooth, round morphology. All particle systems exhibited favorable homogeneity as evidenced by low polydispersity index values (less than 0.20) and were nearly neutral in charge with zeta potentials near zero. Both PTX and imatinib were successfully loaded into the nanoparticles with 50 and 14 weight % loading, respectively. 80% of iRGD was conjugated to the nanoparticles and the peptide showed affinity for A549 lung adenocarcinoma cells *in vitro*. A549 multicellular spheroids were generated to allow for evaluation of the newly developed therapeutics. Finally, *in vitro* analysis using A549 cells showed that the drug-loaded nanoparticles were more effective at killing cells than pure drugs. Overall, this work shows the promise of Ac-Dex drug-loaded nanoparticles conjugated with iRGD to enhance the treatment of lung cancer.

ACKNOWLEDGMENTS

I would like to thank my major professor, Dr. Samantha Meenach, for the opportunity to complete this exciting research with her in an area that I have great passion for. Her advice and support is greatly appreciated. I have enjoyed being taught by her immensely and she is an excellent professor who has inspired me to continue learning with an open and positive mind. I was impressed by her devotion to science research and she was always there when I was faced with difficulties.

I would like to thank my committee members, Dr. Geoffrey D. Bothun and Dr. Wei Lu for their support. Dr. Bothun granted me access to many instruments and equipment and my research would not completed without his assistance. I appreciate the valuable suggestions that Dr. Wei Lu gave me when issues arose with my research. I also want to thank Dr. Arijit Bose, Dr. Everett E. Crisman, Dr. Al Bach, and Dr. Aftab Ahmed for their suggestions and collaborations. Many property owners granted me access to study sites, and their cooperation is appreciated.

Numerous other individuals provided me with assistance that enabled me to complete the research presented in this thesis. Thanks to Zimeng Wang for sharing his thoughts and ideas with me, which were really helpful. I would like to than my fellow graduate students, Matthew Preiss and Aihong Xi, and undergraduate students, Alex Tsoras and Stephanie Geiger, for providing help during my research. The following people provided field and laboratory assistance: Vin Caramadre, Rob D'Ambrosca, and Kim Andrews, and their help was very valuable.

Finally, my family and friends were a great help with their encouragement along the way. I would like to thank Xiao Liu, for bringing me a lot of happiness and

cheering me up when I felt down although he is far away in Los Angeles. Thanks to Yuzi Zhang and my roommates, Hu Yue and Yingnan Dong, for their support. I am especially thankful to my parents, Yubo Sun and Zhufang Lei, for their love as I would not have the chance to do what I love doing without them. Thanks to grandfather for being so brave during his battle with colon cancer.

PREFACE

This thesis was written and formatted following the guidelines presented by the University of Rhode Island Graduate School. There are four chapters: Introduction (Chapter 1), Materials and Methods (Chapter 2), Results and Discussion (Chapter 3), Conclusions and Future Work (Chapter 4), and Appendix. I sincerely hope you enjoy the fruit of my labor as a student in Dr. Samantha Meenach's lab in the College of Engineering.

TABLE OF CONTENTS

LIST OF TABLES

TABLE **PAGE**

LIST OF FIGURES

FIGURE **PAGE**

CHAPTER 1

INTRODUCTION

1.1 Background and Treatment of Lung Cancer

The optimization and improvement of cancer therapeutics is currently an important objective of pharmaceutical research since there are still many problems faced in the treatment of many types of cancer including lung, glioblastoma, and pancreatic cancers, which have extremely poor treatment success rates (Sneed 1998). Therefore, the improvement of cancer treatment options through methods such as targeting and controlled release of therapeutic agents is in great need.

Lung cancer is the second most commonly diagnosed cancer and the most fatal of all types of cancers, accounting for about one out of five malignancies in men and one out of nine malignancies in women (NCI 2014). There are two major types of lung cancer: small cell lung cancer (SCLC), which is also called oat cell cancer because the cells resemble oat grains, and non-small cell lung cancer (NSCLC). The aggressiveness of this disease and treatment options depend on the type and stage of cancer diagnosed. Available treatment options might include surgical resection, chemotherapy, and/or radiation. Since many types of lung cancer grow quickly and spread rapidly, and because the lungs are vital organs, early detection and prompt treatment (usually involving an initial surgery to remove the tumor) is critical to ensure increased patient survivability.

The majority of lung cancers are classified as non-small cell lung cancer, where about half of these are squamous cell carcinomas (SCC). SCC, sometimes called epidermoid carcinoma, is more prevalent in men and arises in the lining of the large air passageways or bronchi. Another common type of NSCLC is adenocarcinoma, which occurs at the outer edges of the lung. A small percentage of NSCLC are large-cell carcinomas, which usually develop in the smaller bronchi. Non-small cell lung cancer that begins at the top of the lung sometimes spreads to the nerves and blood vessels leading to the arm. All three subtypes of NSCLC develop differently and treatment options are often based on the location of the particular cancer and its rate of spread (NCI 2014).

Early diagnosis and intervention can improve the survivability of patients diagnosed with lung cancer. Minimally invasive treatments such as video-assisted thoracoscopy and thoracotomy surgery (VATS) and radiofrequency ablation (RFA) can be used for the detection of lung cancer in its early stages. Comprehensive multi-modality treatment with a combination of local and systemic therapy can maximize the treatment outcome for more advanced-stage lung cancers. These therapies can include chemotherapy, targeted therapy, and rehabilitation.

The five-year survival rates for patients diagnosed with non-small cell lung cancer who are eligible to undergo treatment can be found in **Table 1**. As seen in this figure, even patients who are diagnosed with Stage 1 NSCLC have only a 54% rate of survival after five years. This is often because even though patients diagnosed with Stage 1 cancer tolerate and survive their first round of treatment well, recurrences of

Table 1: Five-year survival rates of patients diagnosed with non-small cell lung cancer (NSCLC) (NCI 2014).

Stage	5 Year Survival Rate
0	Too few cases to evaluate
I	54%
II	35%
IIIA	10 - 15%
IIIB	< 5%
IV	< 2%

the disease are common and more aggressive. Unfortunately, very few patients with Stages IIIB or V NCSLS will be alive five years after their initial diagnosis. These dismal statistics show the importance in improved treatment options for patients diagnosed with NSCLC throughout the course of their disease.

Surgical resection is the standard of care for early stage lung cancer, however, only 25% of patients have resectable disease at the time of diagnosis (Wisnivesky 2005). This can be attributed to the poor health of patients diagnosed with NSCLC as many of these patients are former smokers with other severe health issues such as chronic obstructive pulmonary disease (COPD) and heart disease. In addition, these patients are often of an advanced age, indicating that they are often not healthy enough to undergo aggressive cancer treatments.

In regards to chemotherapeutics, there are several drug classes used in combination with one another as the first-line therapies for many types of NSCLC (Kelly 2001, Schiller 2002). Of these drugs, there are many FDA-approved compounds currently used clinically for the treatment of NSCLC including paclitaxel (Jinhyang 2012) and cisplatin (Zhang 2011). In addition, there are many drugs under investigation for the treatment of NSCLC such as imatinib (Zhang 2003), everolimus (Kochanski 2012), and artesunate (Zhao 2011). While these particular drugs are not yet widely used in the treatment of NSCLC, they are currently approved for the treatment of other types of cancer.

The ability of chemotherapeutics to kill cancer cells depends on their ability to halt cell division. Usually, these types of drugs work by damaging the RNA or DNA that tells the cell how to copy itself in division (Vermeulen 2003). If the cells are

unable to divide, they subsequently die. The faster the cells are able to divide, the more likely it is that chemotherapy will kill these cells, causing the tumor to shrink. This is the main tenant behind how chemotherapeutics work in that they attack rapidly growing cancer cells while sparing the majority of the body's healthy tissues. However, this means that these therapeutics will also attack rapidly growing cells in other parts of the body including hair follicles and gastrointestinal tract.

Chemotherapeutics ultimately induce apoptosis (self-death or cell suicide). Drugs that disrupt mitotic progression, which are commonly referred to as antimitotics, are used extensively for the treatment of cancer. Paclitaxel (Taxol®, Bristol-Myers Squibb Co., Princeton, New Jersey), which belongs to this class of chemotherapy drugs (Marupudi 2007), was originally derived from the bark of Taxus brevifolia (pacific yew tree). The structure of PTX can be seen in **Figure 1**. PTX binds to polymerized tubulin in cells, thereby preventing microtubule formation and promoting microtubule stabilization against disassembly. This in turn inhibits mitosis, and therefore prevents cancer growth.

Imatinib mesylate (also known as simply imatinib, STI571, or Gleevec from Novartis Pharmaceutical Inc.), is a recently FDA-approved drug used for the treatment of chronic myelogenous leukemia and gastrointestinal stromal tumors. The structure of imatinib can be seen in **Figure 2**. Imatinib is an adenosine triphosphate (ATP) analogue, and it competitively binds to and inhibits the oncogene BCR-ABL tyrosine kinase, which results from the chromosomal translocation (Zhang 2003). While traditional cytotoxic cancer treatments such as chemotherapy or radiation therapy kill all dividing cells, imatinib acts on a molecular target by a mechanism that is more

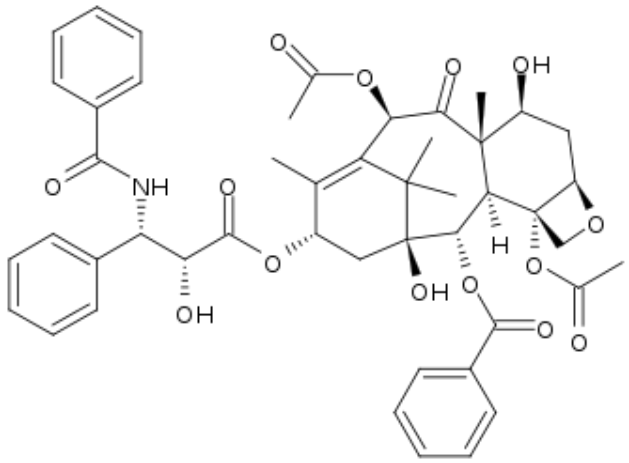

Figure 1: Schematic of the chemical structure of paclitaxel (PTX).

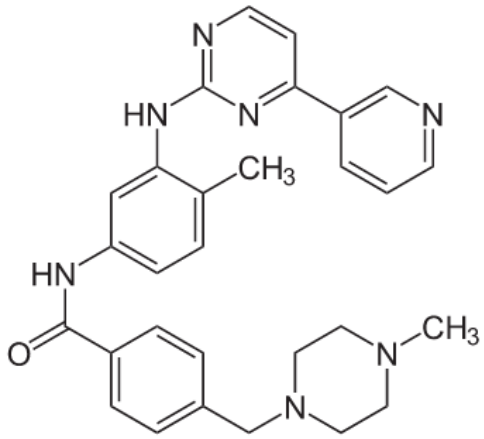

Figure 2: Schematic of the chemical structure of imatinib mesylate (IM).

specific to cancer cells (Timeus 2012). Therefore, it is advantageous to use imatinib for the treatment of cancer because it is more specific to damaging cancer cells, thereby sparing healthy tissue. In particular, imatinib mesylate (IM) has been demonstrated to inhibit the growth and proliferation of gastrointestinal stromal tumors (GIST), and to induce the complete or partial clinical remission in GIST patients. In addition, IM was showed to inhibit the growth of dermatofibrosarcoma protuberans (DFSP) through inhibiting the platelet-derived growth factor (PDGF) receptor (Zhang 2003). Despite encouraging pre-clinical data, IM has had limited clinical efficacy against neuroblastoma tumors when used as a single agent. In regards to lung cancer, it has been demonstrated that A549 cells overexpress PDGF receptor alpha (PDGFR α), one of the known potential targets for imatinib. The inhibitory effect of imatinib on A549 cells is likely mediated through inhibition of this receptor via phosphorylation (Zhang 2003). Overall, these results show the promise that IM has to selectively target and treat a wide variety of tumors.

Despite the widespread use of the aforementioned therapeutics for the treatment of cancer, as with other types of chemotherapeutics, they often face challenges in therapeutic efficacy due to limitations in systemic delivery. In particular, the delivery of paclitaxel faces many challenges due to its lipophilic nature and high protein affinity, which ultimately results in low bioavailability due to its very minimal solubility in water. Also, while the addition of Cremophor EL (a type of polyethoxylated castor oil) and ethanol in the intravenous Taxol® formulation is used to increase the solubility of PTX, these additives often cause severe side effects in many patients (Carvalho 2011).

It has been shown that drug solubilization, an increase in tumor accumulation, and toxicity attenuation of drugs can be enhanced via the use of nanoparticles for the delivery of anti-cancer agents. For example, single-agent paclitaxel plays a central role in the treatment of advanced NSCLC. As mentioned previously, the use of this drug is limited, however, by its poor solubility and by the toxicities associated with additives in the formulation Taxol®. Abraxane is an FDA-approved therapeutic that is comprised of a paclitaxel protein (albumin)-bound nanoparticle system delivered to patients via an injectable suspension. These nanoparticles were developed by American BioScience, Inc. (Santa Monica, California) and are Cremophor EL- and ethanol-free. That nanoparticles are approximately 130 nm size and have been designed to address the solubility limitations of traditional paclitaxel (Green 2006).

In addition, paclitaxel-loaded poly(ethylene glycol) and poly(lactic-co-glycolic acid) (PLGA)-based nanoparticles have been developed where this new system is more cytotoxic on Hela cells than Taxol® (Goodman 2008). In contrast to Cremophor EL, no cytotoxicity of the polymers that make up these nanoparticles was observed (Danhier 2009). In regards to IM, imatinib mesylate has also been successfully loaded into PEG-PLGA nanoparticles as an model system for successful intracellular delivery of molecular targeting drugs in excised veins (Kimura 2008). Similarly, imatinib mesylate-chitosan poly(ε-caprolactone) (PCL) nanoparticles have been investigated for their potential in enhancing controlled release and improving chemotherapeutic efficiency of IM (Cortese 2014). In regards to tandem delivery vehicles, dual-drug loaded nanoparticles containing PTX and gemcitabine have been used against human pancreatic cancer cells and their cytotoxicity was significantly improved compared to

the free drugs (Aryal 2010). A study from the Acharya lab demonstrated that dual-drug loaded nanoparticles work in a synergistic manner lowering the dose of administration and time of action of the drugs, ensuring that both drugs reach the targeted cells specifically and maximize cytotoxicity while minimizing the chances of cell resistance to any one drug (Acharya 2011). Current treatment, however, revolves around the combined delivery of multiple therapeutics, and this is not easily achieved with single-agent nanoparticle systems demonstrating the need for a therapeutic capable of tandem delivery of chemotherapeutics. Overall, these studies show the feasibility in using drug-loaded nanoparticles to enhance the treatment potential of currently available anticancer therapeutics.

1.2 Nanoparticle-Based Drug Delivery Platforms and the Use of Tumor-Penetrating Peptides

There are currently many drug delivery systems in development for the treatment of lung cancer and some of them have achieved moderate progress and have brought about the considerable development in this area of research. In fact, several targeted drug and gene delivery systems have been developed to treat NSCLC more effectively. For example, Sundaram et al. developed a conjugate drug system containing deslorelin (an anti-angiogenic compound) and docetaxel (a traditional chemotherapeutic compound) where the drugs were conjugated with the peptide RGD and delivered *in vivo* (Sundaram 2009). The *in vitro* and *in vivo* efficacy of these peptide-conjugated drugs were evaluated in H1299 (NSCLC) cells and xenografts in athymic nude mice

and the results showed that the conjugated peptide enhanced both the *in vitro* and *in vivo* efficacies significantly.

Nowadays, much attention is being focused on nanotechnology, where this refers to the interactions of molecular components and engineered materials at the nanoscale. Nanomaterials are typically clusters of atoms, molecules, and molecular fragments formed into incredibly small particulates. Nanometer-sized particles have novel optical, electronic, and structural properties that are not always present in individual molecules or bulk solids (Sajja 2009). The concept of nanoscale devices has led to the development of biodegradable self-assembled nanoparticles, which have been engineered for the targeted delivery of anticancer drugs and imaging contrast agents. Nanoconstructs such as these can serve as customizable, targeted drug delivery vehicles capable of ferrying large doses of chemotherapeutic agents or therapeutic genes into malignant cells while sparing healthy cells. Such ‘‘smart’’ multifunctional nanodevices hold out the possibility of radically changing the practice of oncology, allowing easy detection and then followed by effective targeted therapeutics at the earliest stages of the disease (Sinha 2006). In particular, polymeric nanoparticles (PNPs) are defined as particulate dispersions or solid particles with size in the range of 10 - 1000 nm. There has been considerable research interest in the area of drug delivery using particulate delivery systems as carriers for small and large molecules.

The techniques for the preparation of nanoparticles depend on the particular application and or drug to be loaded into the nanoparticle system. A mini-review of several common methods for the preparation of nanoparticles from dispersions of

preformed polymer can be seen in **Table 2** and methods for preparation of nanoparticles from polymerization of monomers in **Table 3**.

Table 2: Review of the common methods used for the preparation of nanoparticles.

Preparation Method	Preparation Details
Solvent evaporation	Solvent evaporation was the first method developed to prepare PNPs. In this method, polymer solutions are prepared in volatile organic solvents and vigorously mixed with aqueous solutions so that emulsions are formulated. This emulsion is converted into a nanoparticle suspension upon evaporation of the solvent from the polymer, which is allowed to diffuse through the continuous phase of the emulsion.
Nanoprecipitation	Nanoprecipitation is also called the solvent displacement method. It involves the precipitation of a preformed polymer from an organic solution and the diffusion of this organic solvent into the aqueous medium in the presence or absence of a surfactant (Fessi 1989, Barichello 1999, Galindo-Rodriguez 2004, Ganachaud 2005) .
Emulsification/solvent diffusion	This method is a modified version of solvent evaporation method. The encapsulating polymer is dissolved into a partially water soluble solvent such as

	propylene carbonate and saturated with water to ensure the initial thermodynamic equilibrium of both liquids. To produce the precipitation of the polymer and the consequent formation of nanoparticles, it is necessary to promote the diffusion of the solvent of the dispersed phase by dilution with an excess of water when the organic solvent is partly miscible with water or with another organic solvent in the opposite case. Subsequently, the polymer-water saturated solvent phase is emulsified in an aqueous solution containing a stabilizer, leading to solvent diffusion to the external phase and the formation of nanoparticles, according to the oil-to-polymer ratio. Finally, the solvent is eliminated by evaporation or filtration, according to its boiling point (Niwa 1993).
Salting out	The salting out method is based on the separation of a water miscible solvent from aqueous solution via a salting out effect. The salting out procedure can be considered as a modification of the emulsification/solvent diffusion (Fessi 1989, Jeon 2000, Jeong 2001, Kostag 2010, Rao 2011) .
Dialysis	Dialysis offers a simple and effective method for

	the preparation of small, narrow-distributed PNP. A polymer is dissolved in an organic solvent and placed inside a dialysis tube with proper molecular weight cut off. Dialysis is performed against a non-solvent miscible with the former miscible. The displacement of the solvent inside the membrane is followed by the progressive aggregation of polymer due to a loss of solubility and the formation of homogeneous suspensions of nanoparticles (York 1999, Kawashima 2001, Rao 2011).
Supercritical fluid technology (SCF)	The need to develop environmentally safer methods for the production of PNP has motivated research on the utility of supercritical fluids as more environmental friendly solvents, with the potential to produce PNPs with high purity and without any trace of organic solvent. Supercritical fluid and dense gas technology are expected to offer an interesting and effective technique of particle production, avoiding most of the drawbacks of the traditional methods. Two principles have been developed for the production of nanoparticles using supercritical fluids: 1) Rapid expansion of supercritical solution (RESS) and 2)

	Rapid expansion of supercritical solution into liquid solvent (RESOLV) (York 1999, Kawashima 2001, Rao 2011).

Table 3: **Overview of the methods used for the preparation of nanoparticles from the direct polymerization of monomers.**

Preparation Method	**Preparation Details**
Emulsion	Emulsion polymerization is one of the fastest methods for nanoparticle preparation and is readily scalable. The method is classified into two categories, based on the use of an organic or aqueous continuous phase. The continuous organic phase methodology involves the dispersion of monomer into an emulsion or inverse microemulsion, or into a material in which the monomer is not soluble (non-solvent). Polyacrylamide nanospheres were produced by this method. As one of the first methods for production of nanoparticles, surfactants or protective soluble polymers have been used to prevent aggregation in the early stages of polymerization (Pinto Reis 2006).
Interfacial polymerization	This method involves step polymerization of two reactive monomers or agents, which are dissolved respectively in two phases (i.e., continuous- and dispersed-phases). A reaction takes place at the interface of the two liquids to form nanoparticles in

	suspension. (Lambert 2000, Charcosset 2006, Gaudin 2008, Wu 2009, Landfester 2010)
Controlled/Living radical polymerization (C/LRP)	Weak intramolecular interactions among polymer chains can be exploited to form organized nanostructured materials, provided the polymers have uniform dimensions, topologies, compositions and functionalities. Particular emphasis is placed on structure–reactivity correlations and ‘‘rules’’ for catalyst selection in atom transfer radical polymerization (ATRP), for chain transfer agent selection in reversible addition-fragmentation chain transfer (RAFT) polymerization, and for the selection of an appropriate mediating agent in stable free radical polymerization (SFRP), including organic and transition metal persistent radicals (Braunecker 2007).

With the increased use of nanoparticles for drug delivery applications, it has been noted that there are many advantages in using these systems over traditional systemically delivered pure drug systems (Kayser 2005, Abhilash 2010). Such advantages in the use of polymeric nanoparticle systems include, but are not limited to the following:

- The increased stability of any volatile pharmaceutical agents present.
- The fabrication of large quantities of particles is easy and cheaply done using a multitude of methods.
- A significant improvement over traditional oral and intravenous methods of administration in terms of efficiency and efficacy is often seen.
- There is delivery of a higher concentration of a pharmaceutical agent to a desired location.
- Modified drug release allows for tailoring of drug delivery.
- They can be applied to a wide variety of drug delivery fields including cancer therapy, delivery of vaccines, contraceptives, and targeted antibiotics.
- The can be easily incorporated into other activities related to drug delivery, including tissue engineering.

The enhanced permeability and retention (EPR) effect involves the extravasation of nanoparticles from “leaky” tumor vasculature into tumor tissue. While the EPR effect has served as the key rationale for using nanoparticles to treat solid tumors, it often does not enable uniform delivery of these particles to all regions of tumor.

Furthermore, while ligands that target cancer cells can often increase the intracellular concentration and cytotoxicity of targeted nanoparticles, the intratumoral penetration is not improved significantly compared with non-targeted nanoparticles (Jain 2010). This is due to multiple factors including ineffective targeting ligands, the tumor-blood vessel wall barrier, slow diffusion into the interstitium of tumors, and physiological barriers of the tumor. These barriers include the lack of functional lymphatic vessels, elevated interstitial fluid pressure, and dense extracellular matrix (Jain 1990).

Tumor-penetrating peptides show great promise in overcoming many barriers that prevent the accumulation and penetration of nanoparticles into the avascular region of tumors. iRGD (internalizing RGD, CRGDKDPDC), a cyclic peptide, has been shown to effectively target and penetrate both *in vitro* three-dimensional multicellular spheroids and *in vivo* animal model tumors when conjugated to drugs or nanoparticles (Sugahara 2010). The peptide iRGD initially accumulates at the surface of αv integrin-expressing cells and tissue in tumors. This is advantageous in that integrins are overexpressed in many types of tumors and tumor-associated vasculature and tissue while being minimally expressed in healthy tissue (Waite 2009, Desgrosellier 2010). Once iRGD reaches the integrin target, it is cleaved by cell surface-associated proteases to expose the C terminus and CandR element which then mediates binding to neuropilin-1, resulting in penetration of the cancerous cells and tissues as seen in **Figure 3**. iRGD has been used effectively with many new and already FDA-approved nanoparticle systems and drugs such as doxorubicin, Abraxane®, Doxil® and trastuzumab to enhance tumor penetration and treatment efficacy in *in vivo* models (Sugahara 2009). In addition, it enhances tumor penetration when co-administered

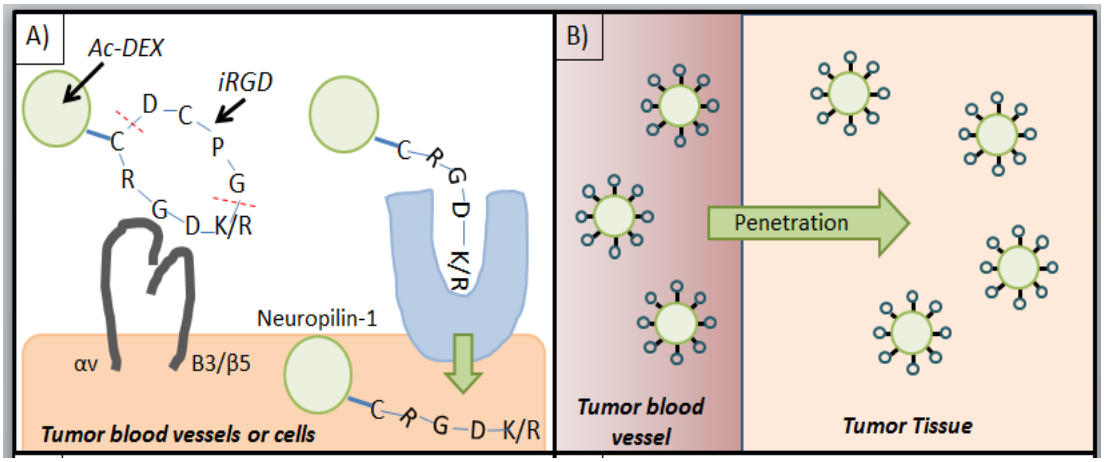

Figure 3: Illustration of iRGD-conjugated acetalated dextran (Ac-Dex) nanoparticles developed in this research where A) depicts the peptide cleavage and penetration mechanism of the iRGD peptide and B) depicts tumor tissue penetration by the nanoparticles due to the presence of iRGD.

with drugs and particles.

The contribution of the therapeutic nanoparticle systems developed in this current research lies in the production of a system that will be easier to deliver to patients by combining multiple agents into one platform. Furthermore, it will allow not only for the direct targeting of anticancer agents to lung tumors but will induce penetration of the nanoparticle into tumor tissue, which can potentially allow for a lower dose of the drugs to be used due to increased specificity (Simberg 2007, Karmali 2009, Ruoslahti 2010). The potential to lower the dosage of chemotherapeutic drugs using a nanoparticle drug delivery system could result in a treatment that is both safer for patients and easier to tolerate, especially for those that are not ideal candidates for aggressive treatment.

Both the elderly and patients with morbidities such as chronic obstructive pulmonary disease (COPD) could benefit greatly from this type of treatment since they are usually neither eligible for surgery nor healthy enough for chemotherapy (Schroedl 2012). Since 50 - 80% of lung cancer patients have COPD (Young 2009), there is a significant portion of the population that could benefit from a more targeted, safer treatment option.

1.3 Multicellular Spheroids (MCS) in Cancer Treatment Evaluation

Determining whether or not nanoparticles will penetrate the tumor microenvironment is often difficult and while cell uptake studies are most commonly used to show this potential, they bear minimal physiological resemblance to tumors.

Conventional two-dimensional (2D) cell culture techniques have been utilized for decades to test the efficacy of anti-cancer therapeutics despite limited translation of the given results into *in vivo* models. The use of three-dimensional (3D) muticellular tumor spheroids (MCS) have been used to overcome these limitations. 3D MCS are clusters of cells that compact to form tight spheroids *in vitro* when cell-to-cell interactions dominate over cell-to-substrate interactions, as seen in **Figure 4**. These systems are advantageous *in vitro* models as they are vastly different from monolayer cultures with respect to gene activation, antigen expression, and growth (Ingram 2010).

MCS can mimic avascular *in vivo* tumors in that they have diffusion limitations for many molecules, including oxygen, and this inefficient mass transport leads to metabolic waste accumulation inside the MCS so that they display a layer-like structure comprised of a necrotic core surrounded by a viable rim of cells (Lin 2008). It is usually the center of tumors that exhibit a hostile microenvironmrnt, as these regions harbor the most aggressive tumor cells, which will regenerate if they are not eliminated. MCS have been effectively used to study many types of therapeutics including nanoparticles, chemotherapeutics, and radiation where the MCS show significant differences in reponse in comparison to 2D cell monolayers (Goodman 2007, Goodman 2008). This illustrates imparts the importance of these systems in optimizing drug and nanoparticle systems for systemic delivery to tumors.

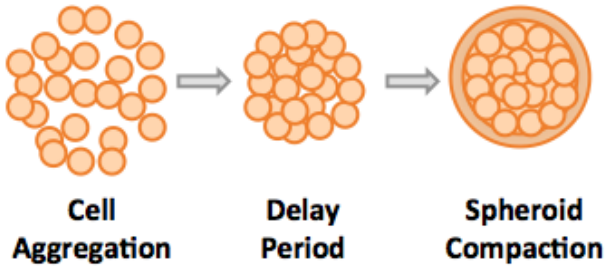

Figure 4: Schematic depicting the formation of spheroids for loose cell aggregates into a compact spheroid following a brief delay period in formation.

1.4 Acetalated Dextran (Ac-Dex) as a Novel Drug Delivery Platform

Acetalated dextran (Ac-Dex) is a newly developed polymer in which pendant acetal groups are reacted onto hydroxyl groups present on the backbone of dextran to give this polymeric compound unique characteristics. The reaction of dextran with 2-methoxypropene leads to the formation of both cyclic and acyclic acetals, causing a switch in solubility and providing a trigger for acid-mediated degradation (Broaders 2009). Cyclic and acyclic acetals have completely different rates of hydrolysis (Fife 1965) and the amount of each present can be tailored by the extent of reaction allowing for the modulation of degradation rates from hour to weeks (Meenach 2012).

In addition to allowing for tunable degradation, Ac-Dex has solubility properties opposite of those of parent dextran, namely that it is soluble in organic solvents and insoluble in water allowing for the processing of Ac-Dex into nanoparticles via standard emulsion techniques (Bachelder 2008). Furthermore, Ac-Dex has pH neutral degradation by-products (parent dextran and small amount of acetone and methanol) and is acid sensitive. At low pH Ac-Dex degradation occurs more quickly whereas at higher pH, the polymer degrades more slowly. *In vitro* assays have indicated that Ac-Dex and its degradation by-products are as safe as the FDA-approved polymer poly(lactic-co-glycolic acid) (PLGA) (Bachelder 2008), which is commonly used in polymeric nanoparticle formulations. The use of Ac-Dex for the tandem delivery of agents significantly advances the development of a targeted biodegradable nanocarrier in that the carrier can be made to degrade fully within a day or up to a week without harmful polymer accumulation or degradation by-products. Thus far, Ac-Dex has been used in particle formulations for applications in immunology/vaccines (Broaders 2009,

Kauffman 2011), tumor targeting (Beaudette 2009), improved storage of therapeutics (Kanthamneni 2012), and pulmonary therapeutics (Meenach 2012).

1.5 Research Aims and Objectives

The overall aim of this project was to develop and optimize acetalated dextran-based peptide-conjugated polymer nanoparticles, which can deliver anti-cancer agents in tandem to allow for enhanced targeting and treatment of non-small cell lung cancer. The specific research for this project include:

- To synthesize acetalated dextran-based iRGD-conjugated nanoparticles loaded with paclitaxel and/or imatinib mesylate.
- To evaluate and optimize the physicochemical properties the peptide-conjugated Ac-Dex nanoparticles.
- To assess the efficiency of the proposed nanoparticle system in the treatment of non-small cell lung cancer using *in vitro* methods.

CHAPTER 2

MATERIALS AND METHODS

2.1 Materials

Phosphate buffered saline (PBS), resazurin (sodium salt, pure, high purity biological stain), glycine, Dulbecco's Modified Eagle Medium (DMEM), and Fungizone® were obtained from Fisher Scientific (Kansas City, MO, USA). Paclitaxel was obtained from LC Labs (Woburn, MA, USA; 99.5% purity). Tween 20, Kolliphore EL (previously known as Cremophor EL), dextran (average molecular weight 9,000 - 11,000), dimethyl sulfoxide (DMSO, ≥ 99.9%), poly(vinyl-alcohol) (PVA, MW 13,000 - 23,000), pyridinium p-toluenesulfonate (PPTS, 98%), fluorescein isothiocyanate (FITC, HPLC grade, ≥ 90%), 2-methoxypropene, deuterium oxide (D_2O), deuterium chloride solution (DCl), dichloromethane (DCM, ≥ 98%), triethylamine (TEA), methanol (HPLC grade, ≥ 99.9%), acetone (HPLC grade, ≥ 99.9%), acetonitrile (HPLC grade, ≥ 99.9%), and fetal bovine serum (FBS) were obtained from Sigma-Aldrich (St. Louis, MO, USA). Imatinib mesylate (Imatinib or IM) was purchased from Adipogen International, Inc. (San Diego, CA, USA). Lysotracker red, calcein AM, ethidium homodimer-1 (EthD-1), sodium pyruvate, and Pen-Strep were purchased from Life Technologies (Carlsbad, CA, USA). Collagen (rat tail type I) was obtained from Discovery Labware, Inc. (Two Oak Park, Bedford, MA, USA). Poly(2-hydroxyethyl methacrylate) (pHEMA) was obtained from Polysciences, Inc. (Warrington, PA, USA). Vectashield hardset mounting media with

4',6-diamidino-2-phenylindole (DAPI) was obtained from Vector Labs, Inc. (Burlingame, CA, USA). All materials were stored in the conditions recommended by the manufacturer and were used as received.

2.2 Synthesis and Characterization of Acetalated Dextran (Ac-Dex)

Ac-Dex was synthesized by the reaction of dextran with 2-methoxypropene as seen in **Figure 5**. 1 g of lyophilized dextran (9,000 - 11,000 MW) was mixed well with 15.5 mg pyridinium p-toluenesulfonate in 10 mL of anhydrous DMSO to allow for complete dissolution of the dry components. The reaction was initiated by adding 1 mL of 2-methyoxypropene, which added the acetal groups (both cyclic and acyclic) to the parent dextran. The reaction proceeded for five minutes to produce fast degrading Ac-Dex (Bachelder 2008, Broaders 2009). The reaction was then quenched with 1 mL of triethylamine (TEA), followed by precipitation in basic water (pH 9.5), isolation via filtration, and lyophilization. Basic water was made by mixing TEA in deionized water for a final pH value of 9.5. This solution prevents the early degradation of pH-sensitive Ac-Dex.

^{1}H-NMR analysis was performed to provide information on the relative cyclic to acyclic ratio of acetal groups of the newly synthesized Ac-Dex polymer. 10 mg of Ac-Dex was suspended in an NMR tube with 700 μL of D_2O (deuterium oxide) and 30 μL of DCl (deuterium chloride), where the DCl was used to facilitate fast degradation of the Ac-Dex in the solution. During the degradation of Ac-Dex, hydrolysis of one cyclic acetal produces one acetone molecule whereas hydrolysis of one acyclic acetal

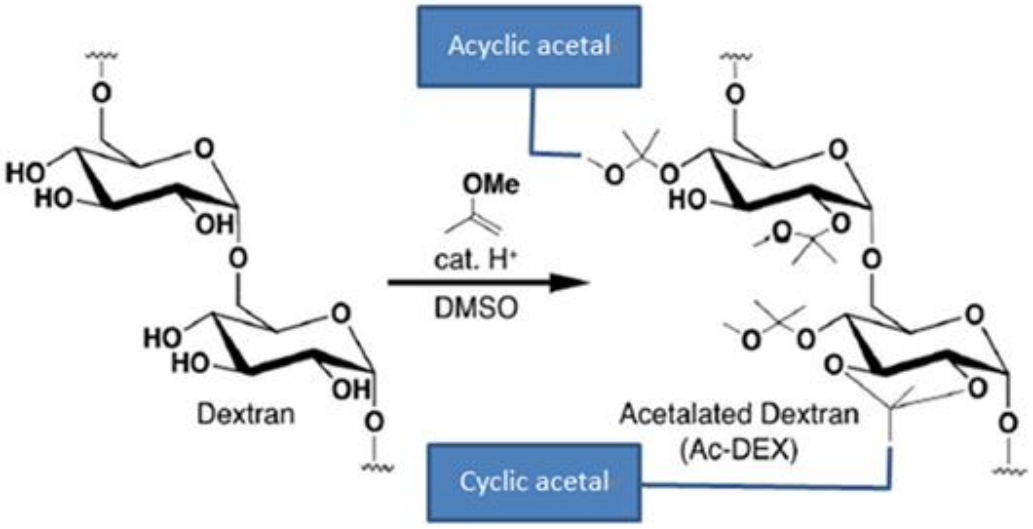

Figure 5: Schematic showing the reaction for the synthesis of acetalated dextran (Ac-Dex). Dextran was reacted with 2-methoxypropene and a catalyst in DMSO to form acyclic and cyclic acetalated dextran.

produces one acetone and one methanol molecule. Therefore, from the relative ratio of the peaks from acetone, methanol, and the cyclic to acyclic ratio of acetal substitution and degrees of hydroxyl substitution per 100 glucose could be determined using ^{1}H-NMR (Broaders 2009). The cyclic to acyclic acetal ratio will be further referred to as the CAC.

2.3 Synthesis, Optimization, and Characterization of Drug-Loaded Ac-Dex Nanoparticles

Single emulsion (water/organic or W/O) nanoparticle synthesis techniques using ultrasonic probe sonication were used to form particles loaded with paclitaxel (PTX) and imatinib mesylate (IM). The initial theoretical encapsulation efficiency for the nanoparticles was 0.1 weight % and 10 weight % for PTX- and IM-loaded nanoparticles, respectively. For PTX-loaded nanoparticles, 0.5 mg of PTX was dissolved into 1 mL of DMSO, which resulted in a concentration of 0.5 mg/mL. For Imatinib-loaded nanoparticles, 50 mg of PTX was dissolved into 1 mL of DMSO, which resulted in a concentration of 50 mg/mL.50 mg of Ac-Dex was then transferred to a 20 mL scintillation vial followed by 900 μL of dichloromethane and 100 μL of the drug/DMSO solution (0.5 mg/ml PTX in DMSO or 50 mg/mL Imatinib in DMSO), resulting in the final organic (O) solution. Then, 2 mL of 3 % w/v poly (vinyl alcohol) (PVA) in phosphate buffered saline (PBS), the aqueous phase (W), was added as to the organic solution and the vial was transferred to an ice bucket. The O and W solutions were sonicated for 30 seconds (QSonica Q500, 0.5 inch flat tip, amplitude of 50 %, 1 second on/off pulse) and then the resulting emulsion was poured into a stirring

solution 40 mL of 0.3 % w/v PVA in PBS and stirred for four hours. After particle hardening and solvent evaporation, the solution containing the nanoparticles was centrifuged at 10,000 rpm (13,571 rcf) for 10 minutes.

After centrifugation, the supernatant solution was decanted and 1 mL of basic water (pH 9.5) was added to each tube. The resulting particle pellets were then resuspended in the basic water using a pipette and water bath sonication, as needed. The remainder of the tubes with the resuspended nanoparticles was filled with basic water and this centrifugation and washing step was repeated until the particles had been washed three times. After the final decantation, the particles were suspended in 1 mL of basic water, and this solution was then transferred to a 5 mL tube. A further 3 mL of basic water was used to rinse the centrifuge tubes and this wash solution was added to the 5 mL tube for a final volume of 5 mL. The particle solution was then put in the freezer for one hour followed by lyophilization for 24 hours. A schematic of this process can be found in **Figure 6**.

The mean size (diameter), polydispersity index (PDI), and zeta potential of the particles was determined using a Malvern Zetasizer Nano ZS capable of dynamic light scattering (DLS) and zeta potential measurement. The shape and surface morphology of particles was evaluated by scanning electron microscopy (SEM), using a Zeiss SIGMA VP Field Emission-Scanning Electron Microscope (FE-SEM). For SEM evaluation, samples were placed on aluminum stubs (TedPella, Inc., Redding, CA, USA) and were then coated with a gold/palladium alloy thin film using an Emscope SC400 sputter coating system at 20 mA for 30 seconds under argon gas. The electron

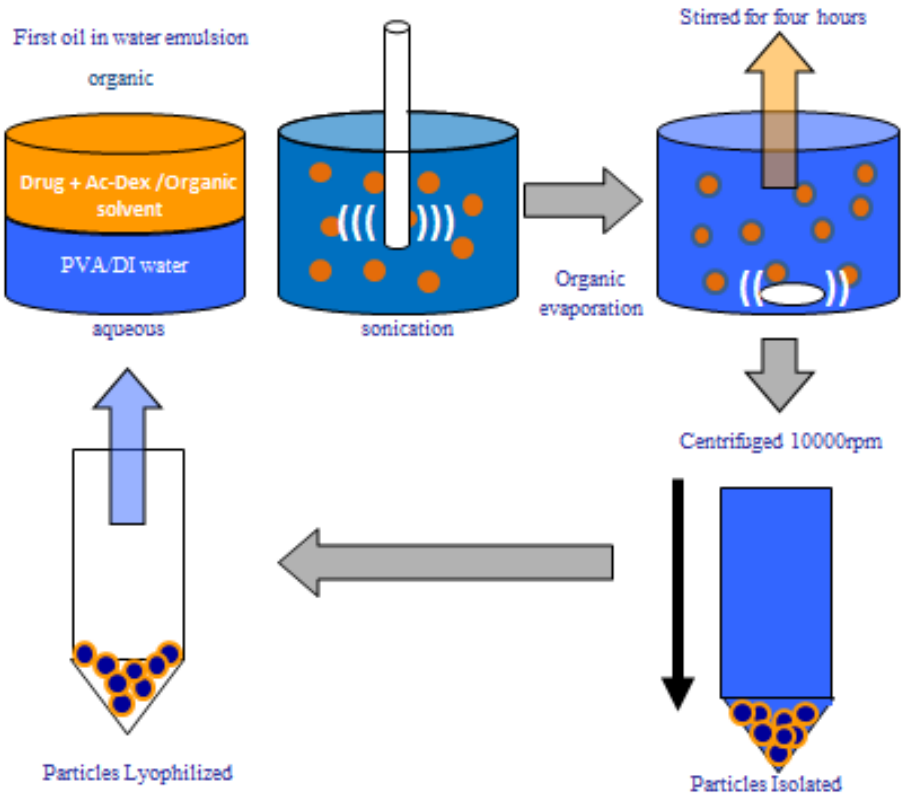

Figure 6: Schematic of nanoparticle synthesis via single emulsion/solvent evaporation method.

beam with an accelerating voltage of 5 to 10 kV was used at a working distance of 13.3 to 15.3 mm. Images were captured at several magnifications.

The encapsulation efficiency, drug loading, and drug release of PTX and IM loaded nanoparticle determined by dissolving the particles completely in acrylonitrile and methanol, respectively, and analyzing these results via Ultra Performance Liquid Chromatography (UPLC). PTX nanoparticles drug release behavior was analyzed by placing the particles in a physiologically buffered modified release medium (pH 7.4) containing PBS, 4 weight % Kolliphore EL, and 2.4 weight % Tween 20 to enhance the solubility of PTX upon release. Imatinib-loaded nanoparticles release behavior was analyzed by placing the particles in a physiologically buffered medium (pH 7.4). The release took place at 37 ℃ and 100 rpm.

UPLC was performed using a Hitachi analytical HPLC system with D-700 HPLC System Manager software for data analysis. The separation was achieved using an Ascentis® C-18 HPLC column (4.6 mm x 15 cm, 5 μm pore size). The mobile phase for paclitaxel detection consisted of acetonitrile and water (50:50 v/v) with a 20 μL injection volume and 1.0 ml/min mobile phase flow rate. The column eluate was evaluated at 227 nm for the detection of paclitaxel in the samples. The mobile phase for imatinib detection consisted of 50 volume % methanol and 50 volume % aqueous formic acid (0.5 volume % in water) with a 20 μL injection volume and 1.2 ml/min mobile phase flow rate. The column eluate was evaluated at 270 nm for the detection of IM in the samples. For both the PTX and IM evaluation, calibration curves (**Figure A1** and **Figure A2**, respectively) were generated using UPLC as described above.

These calibration curves are present in Appendix A. From this analysis the encapsulation efficiency and drug loading of the nanoparticles were evaluated as:

$$\text{Encapsulation Efficiency} = \frac{\text{Actual Mass of Drug in Nanoparticles}}{\text{Theoretical Mass of Drug in Nanoparticles}} \text{ x } 100\%$$

$$\text{Drug Loading} = \frac{\text{Actual Mass of Drug in Nanoparticles}}{\text{Mass of Nanoparticles}}$$

Furthermore, the percent of drug released was evaluated from:

$$\text{Drug Release (\%)} = \frac{M_t}{M_\infty}$$

where M_t is the mass of the drug at time point (t) and $M\infty$ is the mass of drug in sample.

Thermal analysis and phase transition measurements were carried out using a TA Q10 differential scanning calorimetry (DSC) system (TA Instruments, New Castle, DE, USA) with TA Instruments Explorer software and DSC refrigerated cooling accessory. 1 to 5 mg of sample was weighed into hermetic anodized aluminum DSC pans and was sealed hermetically sealed. Dry nitrogen gas was used as the purging gas at 50 mL/min. The heating range during DSC analysis was 0 to 300 ℃ at a heating scan rate of 10.00 ℃/min.

2.4 In Vitro Biological Characterization

Lung carcinoma (A549) cancer cells (obtained from American Type Culture Collection, Manassas, VA, USA) were evaluated for their response to the chemotherapeutic agents paclitaxel and imatinib. The base cell culture medium for the cell line was Dulbecco's Modified Eagle Medium (DMEM). The complete medium for cells contained DMEM with 10 % v/v fetal bovine serum (FBS), Pen-Strep (100 I.U./ml penicillin, 100 μg/ml streptomycin), Fungizone® (0.5 μg/ml amphotericin B, 0.41 μg/ml sodium deoxycholate), and 1 mM of sodium pyruvate. The cells were cultured at 37 ℃ and 5 % CO_2 in a humidified incubator and were used from passages 3 through 15. A549 cells were selected for the described research since these cells have been shown to overexpress αvβ3 integrins (Odrljin 2001, Chetty 2010) and therefore iRGD should home to and penetrate into cells and spheroids composed of these cells (Sugahara 2009).

Initially, for two-dimensional (2D) studies, A549 cells were seeded at 5,000 cells/well with 100 μL/well in 96 well plates and were placed in an incubator for 24 hours. For three-dimensional (3D) multicellular spheroid (MSC) cell studies, 96 round bottom well plates were coated with 0.5 % w/v poly(2-hydroxyethyl methacrylate) (pHEMA) in 200 proof ethanol and allowed to try for 48 hours. A549 cells were then seeded at 5,000 cells/well, 100 μL/well, and with 20 μg collagen/ml in the media in the coated round bottom 96 well plates. These plates were then centrifuged at 1500 rcf for 15 minutes and were placed in the incubator for 24 hours to facilitate spheroid compaction and formation.

The 2D cells and 3D spheroids were then exposed to the following conditions for 48 hours: (i) raw PTX at 0.001, 0.01, 0.05, 0.1 0.5, 5 and 10 μM in complete medium with 0.1 volume % DMSO, (ii) 0.1% PTX-loaded nanoparticles at 0.001, 0.01, 0.05, 0.1, 0.5 and 1 μM, where the PTX amount was calculated from the actual drug loading of the nanoparticles, (iii) raw imatinib at 0.01, 0.05, 0.1, 0.5, 1, 5, 10, 50, and 100 μM in complete medium with 0.1 volume % DMSO, and (iv) 10% imatinib-loaded nanoparticles at 0.01, 0.05, 0.1, 0.5, 1, 5, 10, and 50 μM imatinib, where the IM amount was calculated from the actual drug loading of the nanoparticles. The controls for these studies were complete media with 0.1 volume % DMSO. The media solutions contained 0.1 % (v/v) DMSO to increase PTX and IM solubility and the DMSO control was used as a comparison to ensure no negative effects on the cells were due to the solvent. The solutions were all initially made with double the final concentration and 100 μL of the solutions was added to each well already containing 100 μL of media.

After 48 hours, a resazurin assay was used to assess the cell viability of the cells. Resazurin is converted to highly fluorescent resorufin by cells that are alive. 20 μL of 20 mM resazurin was added to each well containing cells and the well plates were incubated for 3 hours. After this time, the samples were evaluated using a multi-mode plate reader (Cytation 3, BioTek Instruments, Vermont, USA) at an excitation wavelength of 544 nm and emission wavelength of 590 nm with gains of 50, 70, and 90. The relative viability of the cells was determined by the fluorescence intensity:

$$\text{Relative viability (\%)} = \frac{\text{Fluorescence Intensity of Sample}}{\text{Fluorescence Intensity of Control}}\ x\ 100\%$$

As seen above, these results were reported as the ratio of the fluorescence intensity of the resorufin generated from live cells for a given sample exposed to treatment in comparison to the fluorescence intensity generated from live cells not exposed to drug treatment. The inherent relative viability is thus a comparison in cell response to the given control. The corresponding half maximal inhibitory concentration (IC_{50}) values for raw PTX, 0.1% PTX-loaded nanoparticles, raw imatinib, and 10% imatinib-loaded nanoparticles in the sample were determined using the four-parameter logistic equation and were subsequently fit to this equation using http://www.readerfit.com. The four-parameter logistic equation used to generate and fit the dose-response curves corresponding to the relative viability and drug concentration is defined as:

$$V = D + \frac{A - D}{1 + \left(\frac{x}{C}\right)^{B}}$$

where V is the relative viability, A is minimum viability of the cells at the highest tested drug concentration, B is the Hill's slope of the dose-response curve, C is the IC_{50} value (evaluated at the inflection point of the slope), and D is the maximum viability of the cells not exposed to any therapeutics. The actual viability values were

graphed along with the theoretical fit values obtained from the four-parameter logistic equation.

To evaluate the potential uptake of nanoparticles into lung cancer cells, A549 cells were seeded at 125,000 cells/mL (300 μL/well) in 8 well chamber slides and were placed in an incubator for 24 hours to allow time for cell attachment. The cells were then exposed to 1 mg/mL of fluorescently-labeled drug-loaded nanoparticles in media for 24 hours at 37 ℃. These nanoparticle systems were 0.1% PTX-loaded and 10% imatinib-loaded nanoparticles with the addition of 2 weight % fluorescein isothiocyanate (FITC) added to the organic phase during nanoparticle synthesis to allow for fluorescent imaging of the particles. After the cells were exposed to the nanoparticle/media solutions (up to 24 hours), the particle solutions were removed and the cells were washed twice with 200 mM glycine to remove any unbound particles, followed by an additional wash with PBS. The cells were then stained with 750 nM Lysotracker Red and fixed with hardset Vectashield containing DAPI prior to imaging with a Nikon Eclipse E600 upright microscope.

The ability of A549 cells to form spheroids and their growth with time was evaluated using brightfield microscopy (Nikon Diaphot TMD). The spheroids were imaged immediately after centrifugation and then each day for up to 5 days. The size of the spheroids was analyzed using ImageJ software (Abramoff 2004).

2.5 iRGD Conjugation and Tumor-Penetration Efficacy of Nanoparticles

Two types of iRGD were used for the studies described in this research. The first type of iRGD was peptide with no fluorescent tag and extra cysteine (G) residues that was synthesized, purified (99 % purity), and characterized by Rakesh Tiwari, a collaborator in the Department of Biomedical and Pharmaceutical Sciences at the University of Rhode Island (Kingston, RI). The final compound (NH_2-CGGGCRGDKGPDCG-$CONH_2$) was an alkoxyamine-functionalized peptide that could be conjugated to Ac-Dex nanoparticles owing to the ability of polysaccharides to form stable oxime conjugates with alkoxyamine-bearing molecules (Beaudette 2009). The second type of iRGD use in the described studies was CRGDKGPDC labeled with a TAMRA fluorophore to allow for easy detection of the iRGD in solution. This compound was generously donated by Anastasia Kruse, a collaborator in the Department of Chemical Engineering at the University of Kentucky (Lexington, KY).

As depicted in **Figure 7**, iRGD-conjugated nanoparticles were prepared by mixing 5 mg of the alkoxyamine-functionalized iRGD with 1 mg of Ac-Dex nanoparticles in 1 mL PBS. First, 5 mg of iRGD and 1 mg of nanoparticles was measured into 1 mL of PBS and was then sonicated in a water bath for 15 minutes. The samples were then put on a shaker at 37°C and 100 rpm for 2 days. After 2 days, the samples were centrifuged at 12,000 rcf (10629 rpm) for 15 minutes and the supernatant was removed. The particles were washed twice with 1 mL fresh PBS and then resuspended using sonication. 100 µL/well of particle solution was added to each

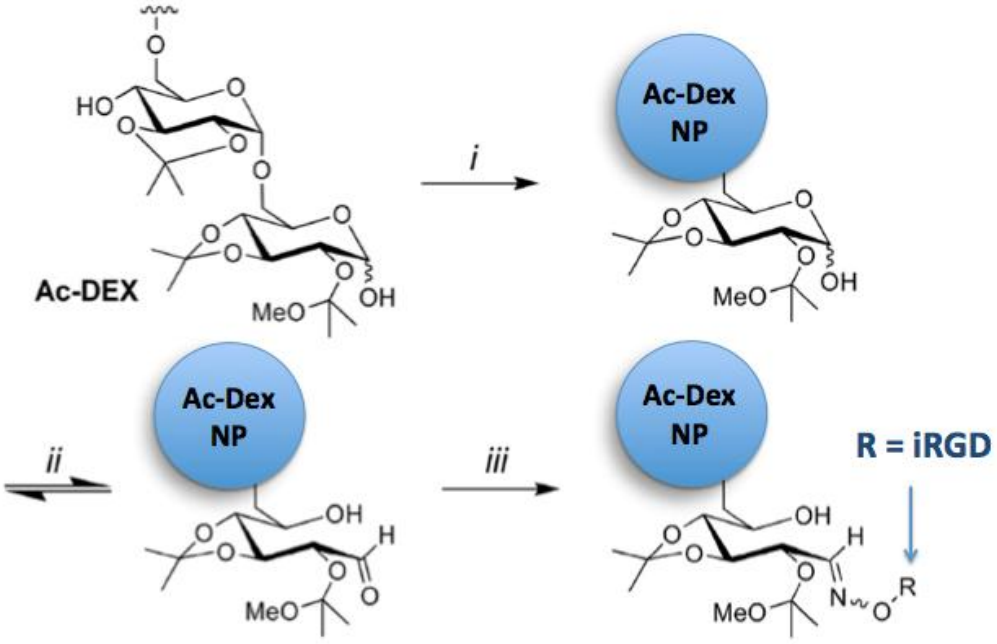

Figure 7: Schematic depicting (i) the formation of Ac-Dex into Ac-Dex nanoparticles (NP), (ii) reducing end chain equilibrium between hemiacetal and straight-chain forms, and (iii) reaction of the reducing end aldehyde with alkoxyamine-conjugated iRGD.

well of a 96 well UV transparent plate and then 300 μL of 20 mg/mL of fluorescamine in acetone was added to each well make the total volume 400 μL. The fluorescamine reacts with primary amines in the iRGD to allow for the quantification of the amount of iRGD present in solution. The amount of iRGD conjugated to the nanoparticles was then evaluated using a fluorescence spectroscopy plate reader (Biotek Cytation3) at an excitation wavelength of 400 nm, emission wavelength of 460 nm, and gain of 100 following one hour of incubation.

To allow for the quantification of the amount of TAMRA-iRGD present on nanoparticles or cells, a calibration curve of TAMRA-iRGD was prepared in media without serum as seen in **Figure A3**. Concentrations of 0, 0.0005, 0.0025, 0.00375, 0.005, 0.0125, 0.025, 0.0375, 0.05 mg/mL were prepared and 100 μL of each concentration/solution was added to a 96 well plate. The fluorescence of the solutions was then read using an excitation wavelength of 540 nm and emission wavelength of 585 nm (gain values of 50, 75, and 100) using the Biotek Cytation3 plate reader.

To evaluate the affinity of TAMRA-iRGD nanoparticles to A549 lung adenocarcinoma cells, cells were seeded at 200,000 cells/mL (100 μL/well) in 96 wells plates and placed in an incubator for 24 hours. The cells were then exposed to different concentrations of TAMRA-iRGD in media including 0, 0.0005, 0.0025, 0.00375, 0.005, 0.0125, 0.025, 0.0375, 0.05 mg/mL in serum-free media. At different time points (0, 0.5, 1, 2, 4, 7 and 24 hours), the area-average fluorescence of the samples was evaluated at an excitation wavelength of 540 nm and emission wavelength of 585nm with a gain of 100 using the Biotek Cytation3 plate reader. Prior

to analysis at each time point, the iRGD solution was removed from the wells and the cells were washed three times with PBS to remove any unbound iRGD.

CHAPTER 3

RESULTS AND DISCUSSION

3.1 Characterization of Acetalated Dextran (Ac-Dex)

Because of the significant differences in the rates of hydrolysis between the acyclic and cyclic acetals present on Ac-Dex, it is important to know the cyclic acetal coverage (CAC) of Ac-Dex to ensure that the degradation will be appropriate for the given application. The relative proportion of cyclic and acyclic acetals was determined by comparing the relative concentrations of acetone and methanol present during ^{1}H-NMR analysis. This is possible since the hydrolysis of one acyclic acetal yields one molecule each of acetone and methanol, whereas the hydrolysis of one cyclic acetal yields only a single acetone molecule (Bachelder 2008). The CAC was then determined via the ratio of acetone to methanol by comparing the integration of the acetone peak (2.08 ppm) to the methanol peak (3.34 ppm) from ^{1}H-NMR analysis. All integrations were normalized to the number of protons on each molecule. The calculation protocol for this method can be found in **Appendix B**.

Analysis of Ac-Dex formed after a 5-minute reaction period was completed via ^{1}H-NMR (see **Figure 8**). These results showed that the cyclic acetal coverage (CAC) of the fast degrading Ac-Dex was approximately 70%. In addition, the conversion of hydroxyl groups on the parent dextran to acetal group was at least 80% for all batches

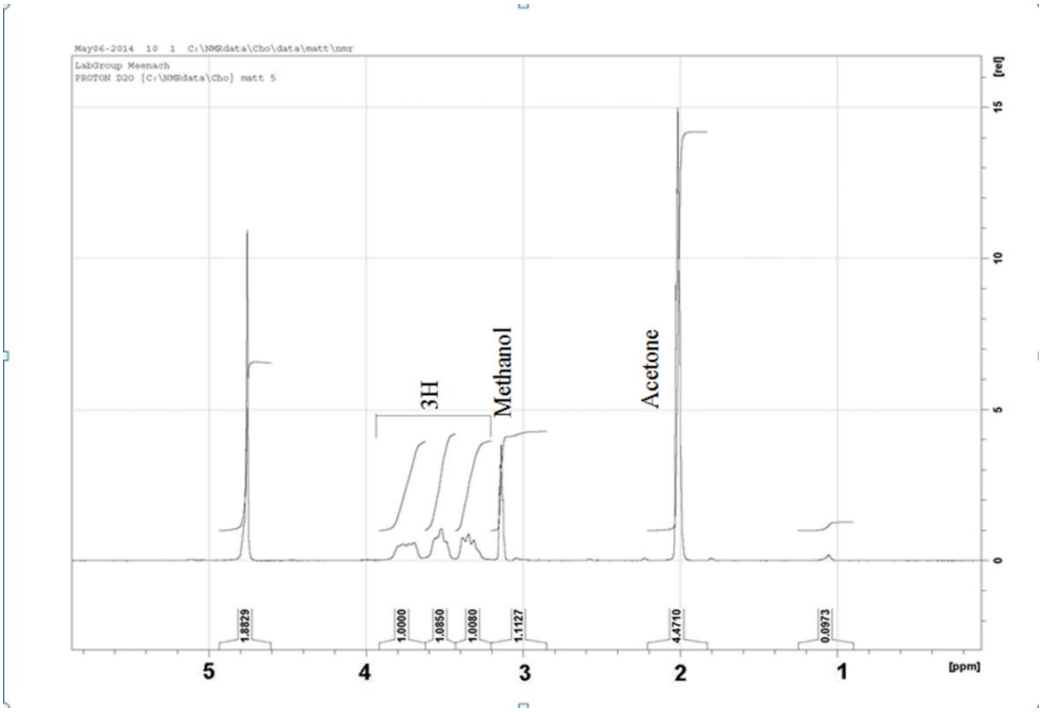

Figure 8: Representative NMR spectra of acetalated dextran use for cyclic acetal coverage (CAC) calculations.

of Ac-Dex, indicating good coverage of acetals on the polymer backbone. The reported CAC value is appropriate for the desired application as Ac-Dex with this property is known to degrade with a few days (Bachelder 2008, Bachelder 2008, Meenach 2012), which is appropriate for the application of nanoparticles to tumors.

3.2 Characterization of Drug-Loaded Ac-Dex Nanoparticles

The size (diameter), polydispersity index (PDI), zeta potential, encapsulation efficiency, and drug loading of the nanoparticles was evaluated to show the feasibility and efficacy of using the emulsion/solvent evaporation method for the generation of chemotherapeutic nanoparticles. The size of both blank (no drug) and drug-loaded Ac-Dex nanoparticles was evaluated using dynamic light scattering (DLS) and the results are depicted in **Table 4**. The particles sizes range from 232 to 282 nm, which is suitable for nanoparticles used in the applications for the systemic delivery of nanoparticles and cancer treatment via tumor penetration and controlled delivery.

Nanoparticle formulation and surface morphologies were visualized and analyzed via scanning electron microscopy (SEM) as seen in **Figure 9**. From these images it can be seen that the nanoparticles are smooth and spherical, which is appropriate for the indicated application. From these images it can be estimated that the diameters of both the blank and drug-loaded nanoparticles range from 200 to 300 nm, confirming the results gained from the DLS analysis. Finally, no differences were seen between systems with paclitaxel (PTX), imatinib mesylate (IM), and blank nanoparticles regarding their morphology, indicating the loading of the drug had little effect on these

Table 4: Physicochemical characterization results for blank and drug loaded nanoparticles including particle diameter, polydispersity index (PDI), zeta potential, encapsulation efficiency, and drug loading (μg drug/mg nanoparticles). Data represents average values ± standard deviation for at least n = 3.

Particle System	Diameter (nm)	PDI	Zeta Potential (mV)	Encapsulation Efficiency (%)	Drug Loading (μg drug/mg NP)
0.1% PTX	232 ± 13	0.21 ±0.08	-0.40 ± 0.02	50 ± 17	0.5 ± 0.17
10% Imatinib	282 ± 2	0.20 ± 0.02	-0.30 ± 0.03	14 ± 3	14 ± 3
Blank	255 ± 25	0.19 ± 0.02	-2.43 ± 0.13	----	----

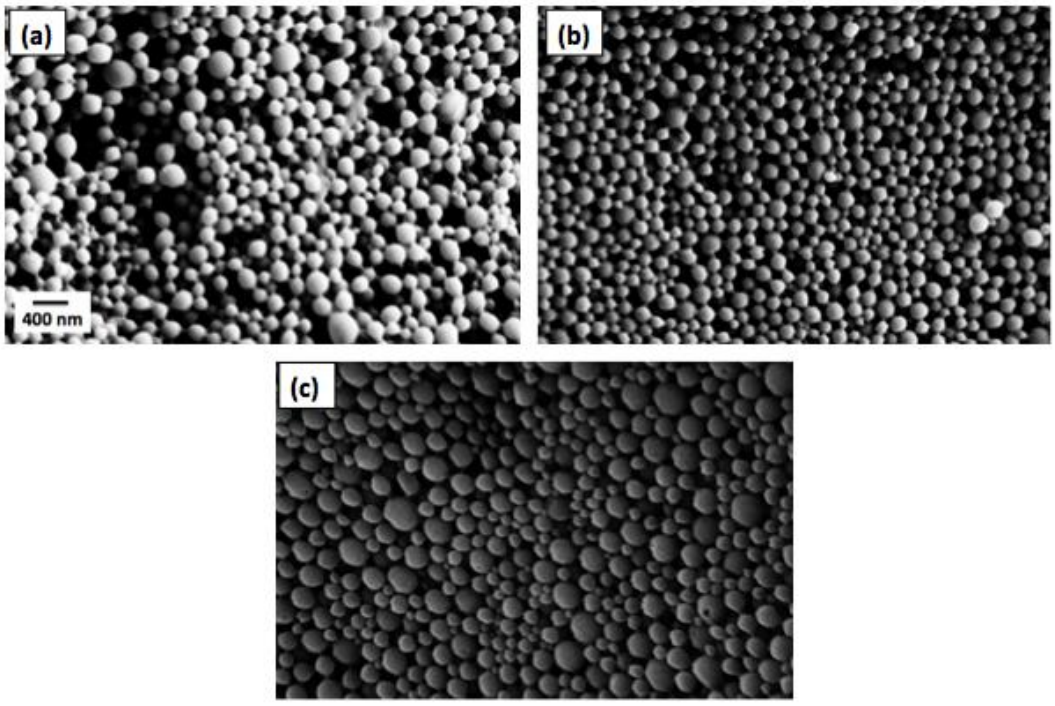

Figure 9: Scanning electron micrographs of (a) 0.1% PTX, (b) 10% imatinib, and (c) blank acetalated dextran nanoparticles.

characteristics in comparison to blank particles without drug.

The polydispersity index (PDI) values from **Table 4** were approximately 0.20, indicating that the nanoparticles, regardless of the presence or type of drug in the nanoparticle systems. In addition, the zeta potential values of the nanoparticles ranged from -2.43 to -0.30 mV, indicating that the particle systems are all nearly neutral (Honary 2013, Honary 2013), with drug loading have no effect on this parameter.

The encapsulation efficiency of the nanoparticles was 50 % for 0.1% PTX nanoparticles and 14 % for 10% imatinib nanoparticles. This ultimately resulted in an actual drug loading of 0.52 μg of PTX per mg of nanoparticles and 14 μg of imatinib per mg of nanoparticles. Overall, these results indicate that both PTX and imatinib can be successfully loaded into Ac-Dex based nanoparticle systems using the emulsion/solvent evaporation particle formation method. In addition, it seems that there is some effect on drug loading due to either the type of drug loaded or the amount of drug loaded into the nanoparticle systems. This could be due to the hydrophobicity or lipophilicity of the drugs present in the nanoparticle systems.

Figure 10 shows the results from differential scanning calorimetry (DSC) for the nanoparticle systems and raw components that made up the nanoparticles. While, the nanoparticles were evaluated a large temperature range, these results ultimately show that the nanoparticles are stable within a normal temperature range that nanoparticles would be exposed to during synthesis, storage, and administration (4 to 100 ℃).

The release of paclitaxel and imatinib from acetalated dextran nanoparticles was evaluated over 48 hours as seen in **Figure 11** (for paclitaxel nanoparticles) and **Figure**

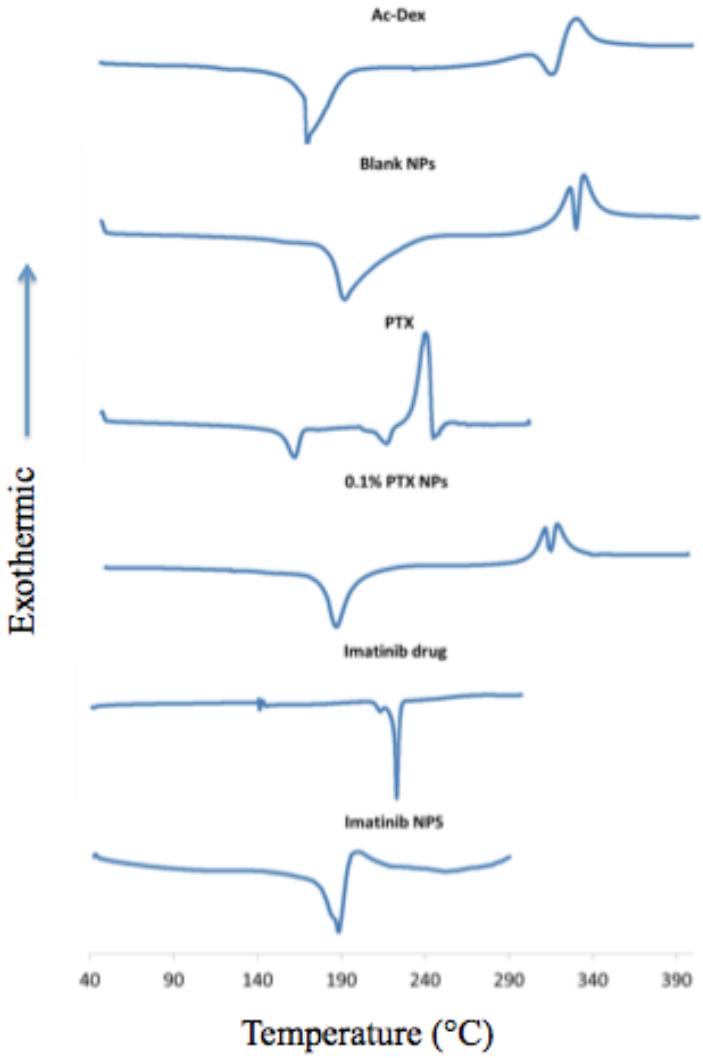

Figure 10: Differential scanning calorimetry (DSC) thermogram of raw acetalated dextran (Ac-Dex), blank nanoparticles without drug (Blank NPs), raw paclitaxel (PTX), 0.1% PTX-loaded nanoparticles (0.1% PTX NPs), raw imatinib, and 10% imatinib-loaded nanoparticles (Imatinib NPS).

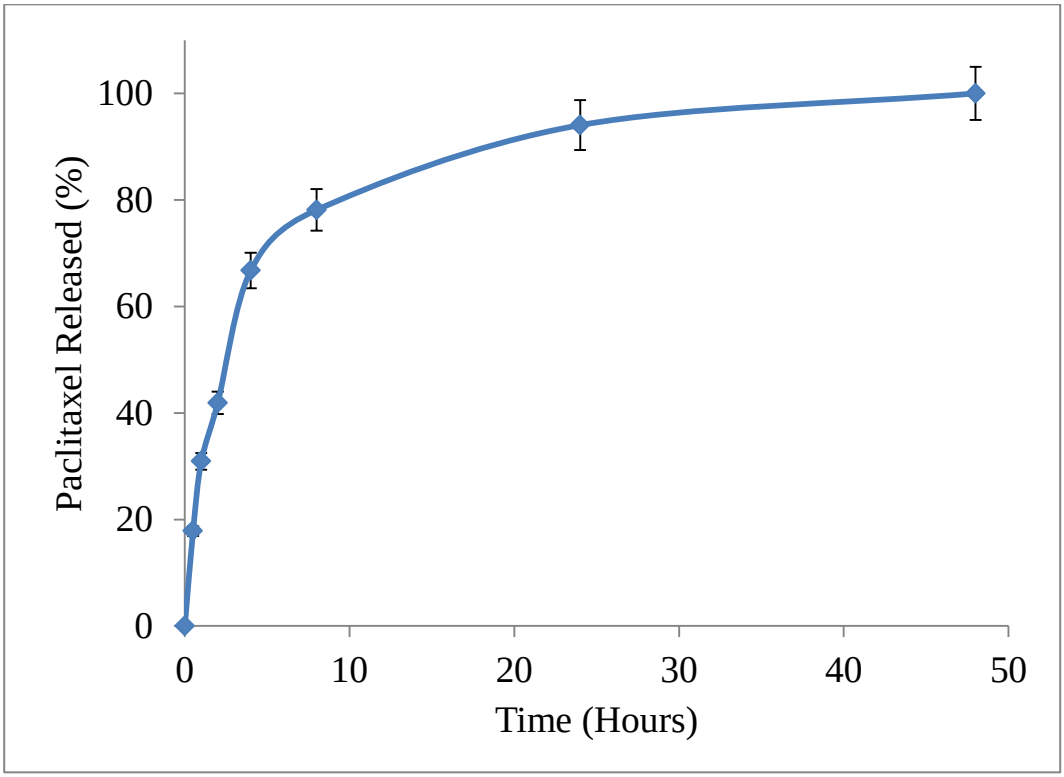

Figure 11: Amount of paclitaxel released versus time for 0.1% PTX nanoparticles.

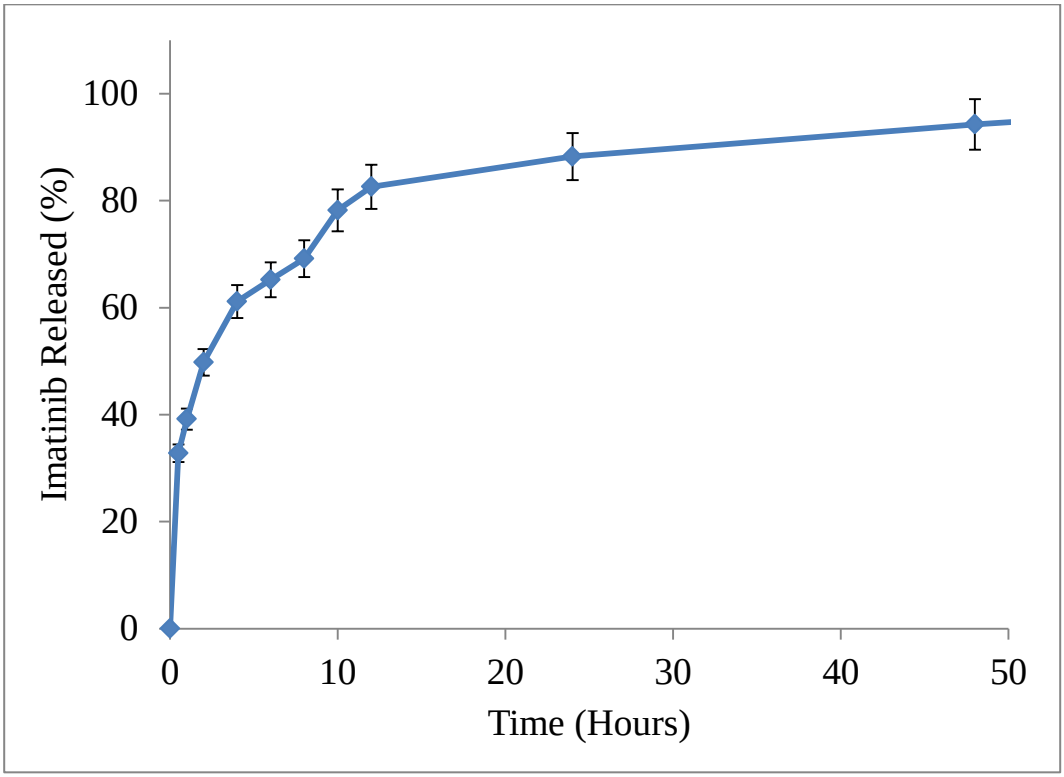

Figure 12: Amount of imatinib released versus time for 10% IM nanoparticles.

12 (for imatinib nanoparticles). The release data shows that the drug-loaded nanoparticles (both PTX and imatinib) exhibited a burst release for the first two hours with 40 % released from PTX-loaded nanoparticles and 60 % released from IM-loaded nanoparticles during this time. Both systems then demonstrated controlled release after the first two hours and the final release for both systems was completed within 48 hours.

Overall, these results demonstrate the feasibility in synthesizing PTX and IM-loaded nanoparticles with Ac-Dex as the polymer. The systems ultimately exhibit the desired morphological, size, charge, and shape necessary for systemic delivery to tumors and are stable at the desired working temperatures. Furthermore, the nanoparticles exhibit the ability to control the release of either PTX or IM for an extended amount of time, which can enhance the efficacy of using these systems in the treatment of lung cancer.

3.3 In Vitro Biological Characterization

The effect of raw paclitaxel, paclitaxel-loaded nanoparticles, and blank nanoparticles on the viability of A549 lung adenocarcinoma cells was evaluated 48 hours after drug and/or nanoparticle exposure. The effect of raw PTX, PTX-loaded nanoparticles and raw Imatinib on A549 cells can be seen in **Figure 13** and **14**. For both the pure drug and PTX nanoparticles, the cell viability decreased with increasing drug concentration as expected. Furthermore, the relative viability of A549 cells exposed to PTX-loaded nanoparticles was lower than that for pure PTX. This

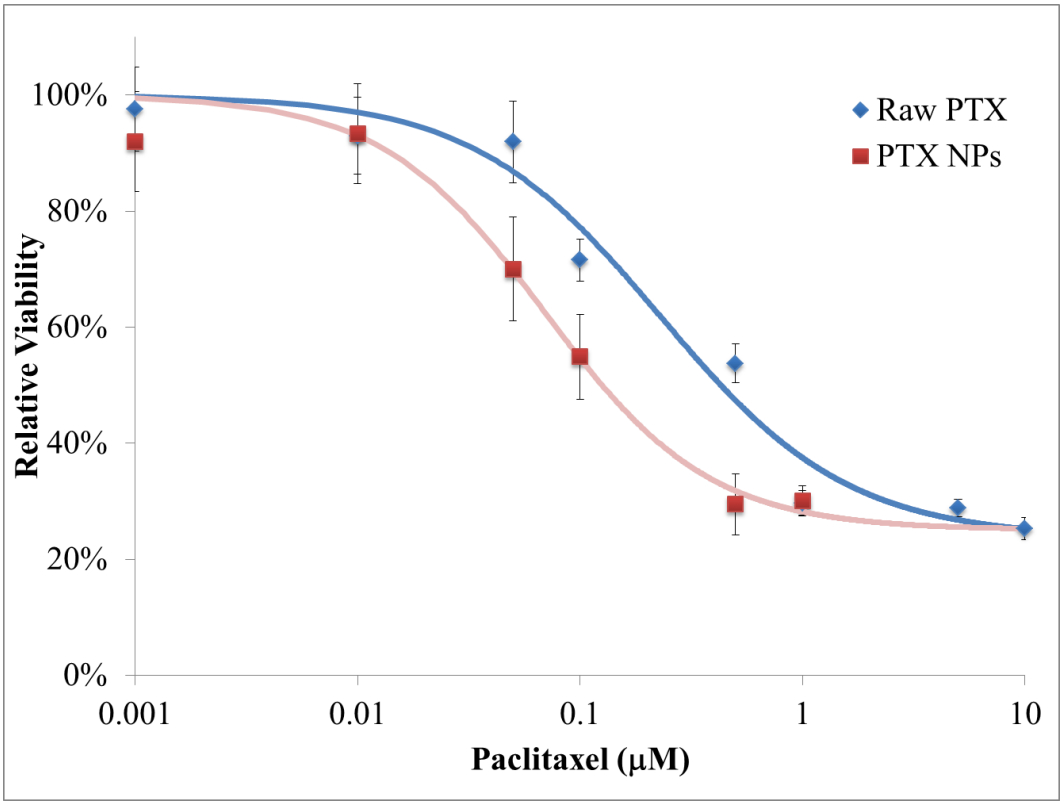

Figure 13: Dose-response curve for A549 cells exposed to PTX and 0.1% PTX-loaded nanoparticles.

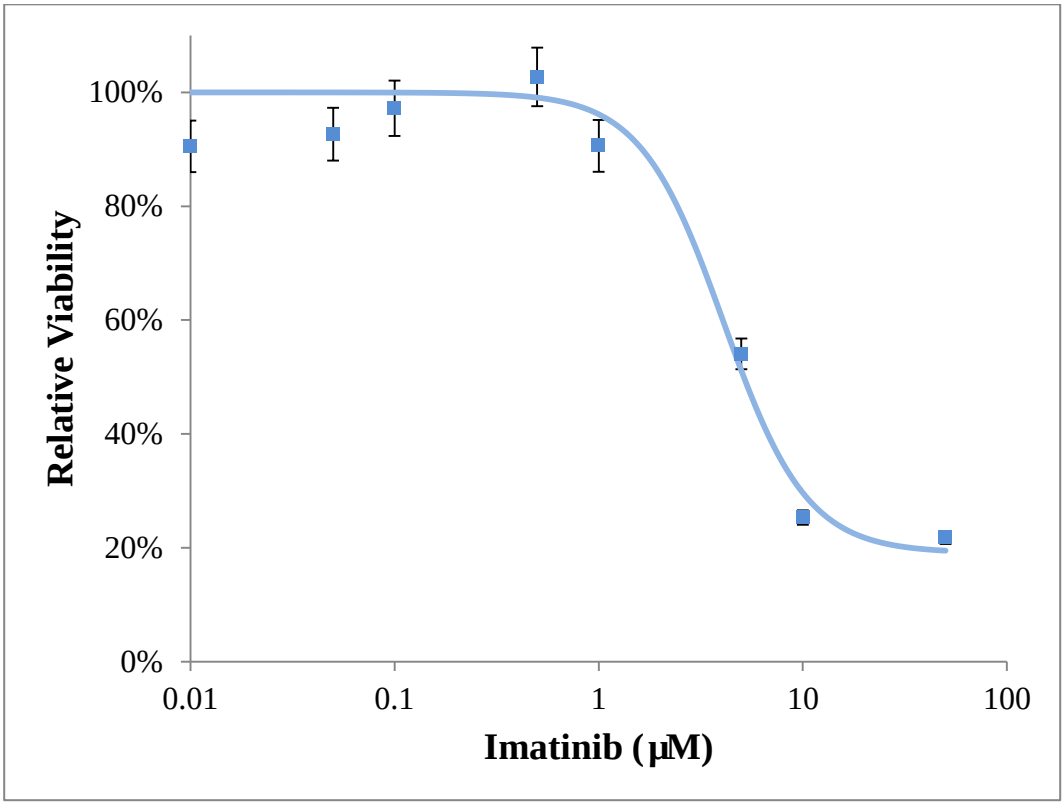

Figure 14: Dose-response curve for A549 cells exposed to Imatinib.

indicated that it takes a lower concentration of drug in the nanoparticles to kill the same number of cells as compared to the pure PTX. This is also indicated by the IC50 values, were the IC50 value for raw PTX was 0.2299 μM and for PTX NPs was 0.0695 μM. This ultimately indicates that the PTX-loaded nanoparticles are more effective in killing lung cancer cells than pure PTX, even without iRGD conjugation. And the IC50 of raw Imatinib was 4.0993 μM.

The effect of blank nanoparticles on A549 cells was also evaluated. The amount of nanoparticles loaded into media for exposure to the cells was determined by using the largest mass of nanoparticles needed for the highest concentration of PTX. The relative viability of cells exposed to blank nanoparticles was 96 %, indicating that the nanoparticle exert minimal to no cytotoxic effects on A549 cells. This, in turn, demonstrates that they should be safe for administration of anticancer therapeutics.

The potential for Ac-Dex nanoparticles to be uptaken into A549 cells was evaluated. For these initial studies, FITC-loaded nanoparticles with no drug were evaluated by exposing the cells to nanoparticles for 5 hours. **Figure 14** shows that after 5 hours the A549 cells exhibited very minimal uptake of FITC-loaded nanoparticles. This could potentially be attributed to the short exposure time or the lack of peptide targeting for these nanoparticles since no iRGD was conjugated onto the nanoparticle surfaces.

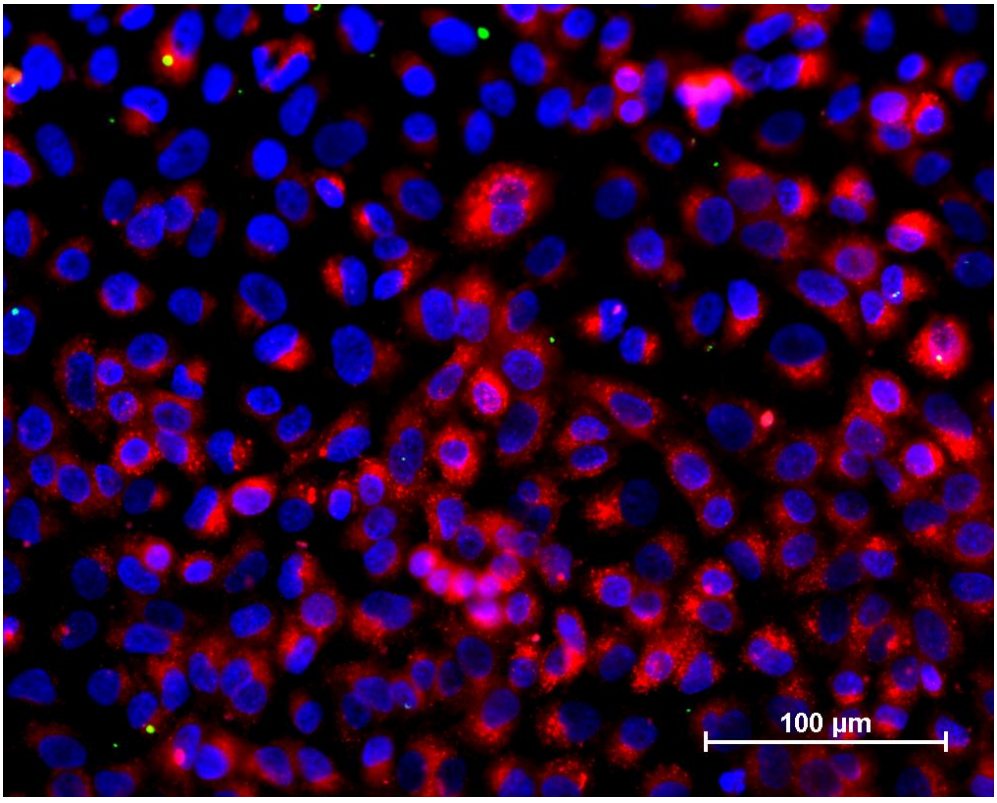

Figure 15: Representative fluorescent image from uptake studies where A549 lung adenocarcinoma cells were exposed to FITC-loaded nanoparticles for 5 hours. The blue fluorescence indicates the cell nuclei, red indicates cellular lysosomes, and green indicates the uptaken nanoparticles.

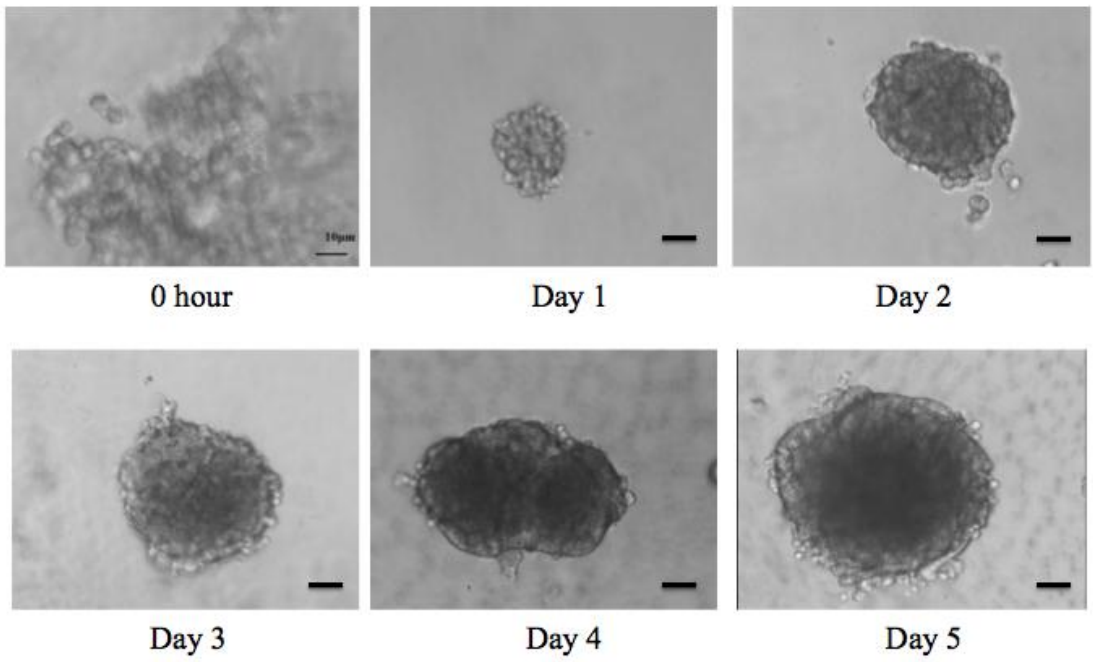

Figure 16: Bright field images of three-dimensional multicellular spheroids comprised of A549 lung adenocarcinoma cells via centrifugation. The scale bar for 0 hour is 10 μm whereas the scale bar for Days 1 through 5 is 100 μm.

3.4 Three-Dimensional Multicellular Spheroid Evaluation

Three-dimensional (3D) multicellular spheroids (MCS) comprised of A549 lung cancer cells were successfully formed using a modified centrifugation technique. In this technique, cells in a small amount of collagen were seeded into non-adherent round bottom 96 well plates followed by mild centrifugation. As shown in **Figure 15**, immediately after centrifugation (0 hour), the cells formed a two-dimensional (2D) confluent monolayer on the bottom of the round bottom well plates. Within 24 hours (Day 1 image) 3D MCS have formed and continue to grow with time. These spheroids show spherical morphology with a high density of cells within their structure.

The size of the spheroids was analyzed by using the brightfield images and ImageJ software. As seen in **Figure 16**, the size of the spheroids increased with culture time and the spheroids reached a diameter of approximately 560 μm after 5 days. Overall, these results indicate the successful formation of A549 multicellular spheroids where these systems will be used in future studies relating the tumor-penetrating nanoparticles.

3.5 iRGD-Nanoparticle Conjugation and Affinity to A549 Cells

The amount of iRGD capable of conjugating to acetalated dextran nanoparticles was determined using the fluorescamine assay. These results indicated that approximately 5.618×10^4 molecules of iRGD were conjugated to each nanoparticle and the iRGD coverage is 0.287 iRGD/nm^2. Overall, these results show that acetalated

dextran nanoparticles can be produced that will be capable of tumor homing and penetration through the iRGD tumor penetrating mechanism.

The affinity of iRGD to A549 cells was evaluated by exposing these cells to differing concentrations of TAMRA-conjugated iRGD for different times (up to 24 hours). These results are indicated in **Figure 17,** which showed that iRGD interacts with and likely penetrates A549 lung adenocarcinoma cells. In this figure, fluorescence intensity of the TAMRA-iRGD attached to the cells is compared to the iRGD concentration and exposure time. After 3 hours, the fluorescence intensity of the samples was the highest regardless of iRGD solution concentration. This indicates that this is the optimal time period for A549 cells to interact with and uptake iRGD, which will be useful in designing future *in vitro* experiments with respect to exposure time. Overall, the fluorescence intensity of the samples increased with increasing TAMRA-iRGD concentration. This is expected because there is a linear relationship between the concentrations of iRGD in serum-free media with respect to fluorescence intensity as shown by the calibration curve in **Figure A3** (see Appendix A). Overall, these studies show the feasibility in using iRGD-conjugated nanoparticles to target A549 lung adenocarcinoma cells for the enhanced treatment of lung cancer.

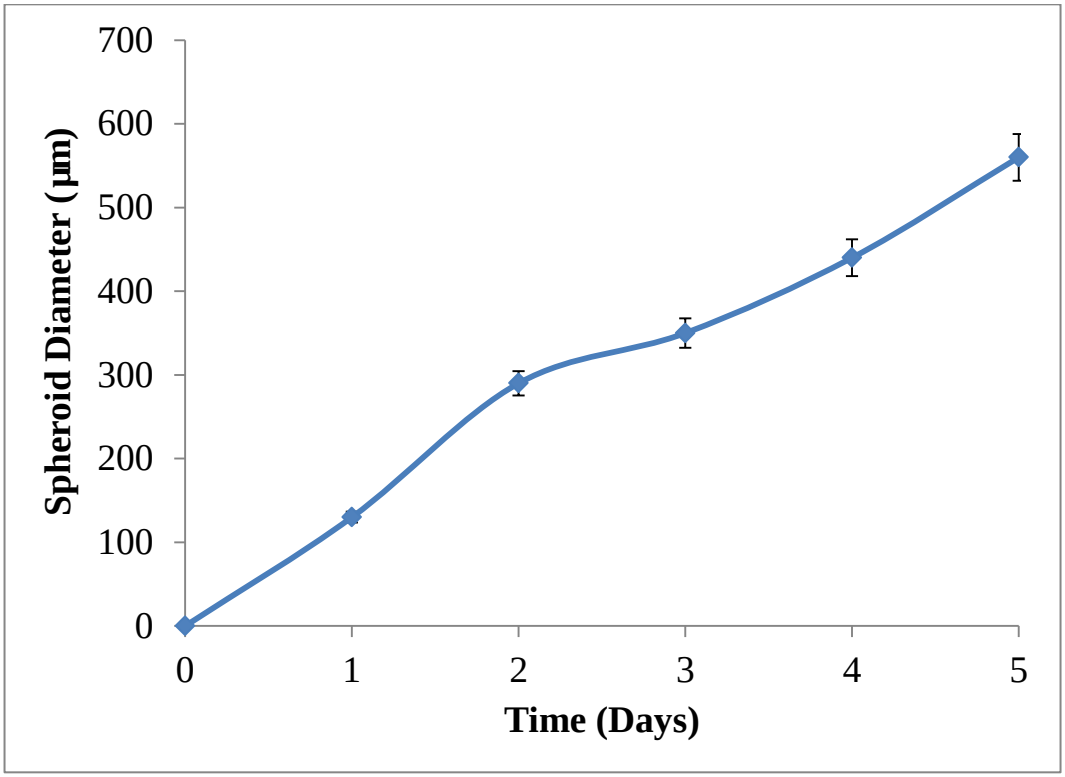

Figure 17: Diameter of three-dimensional multicellular spheroids with respect to time. The diameter of the spheroids was evaluated using brightfield images and ImageJ software.

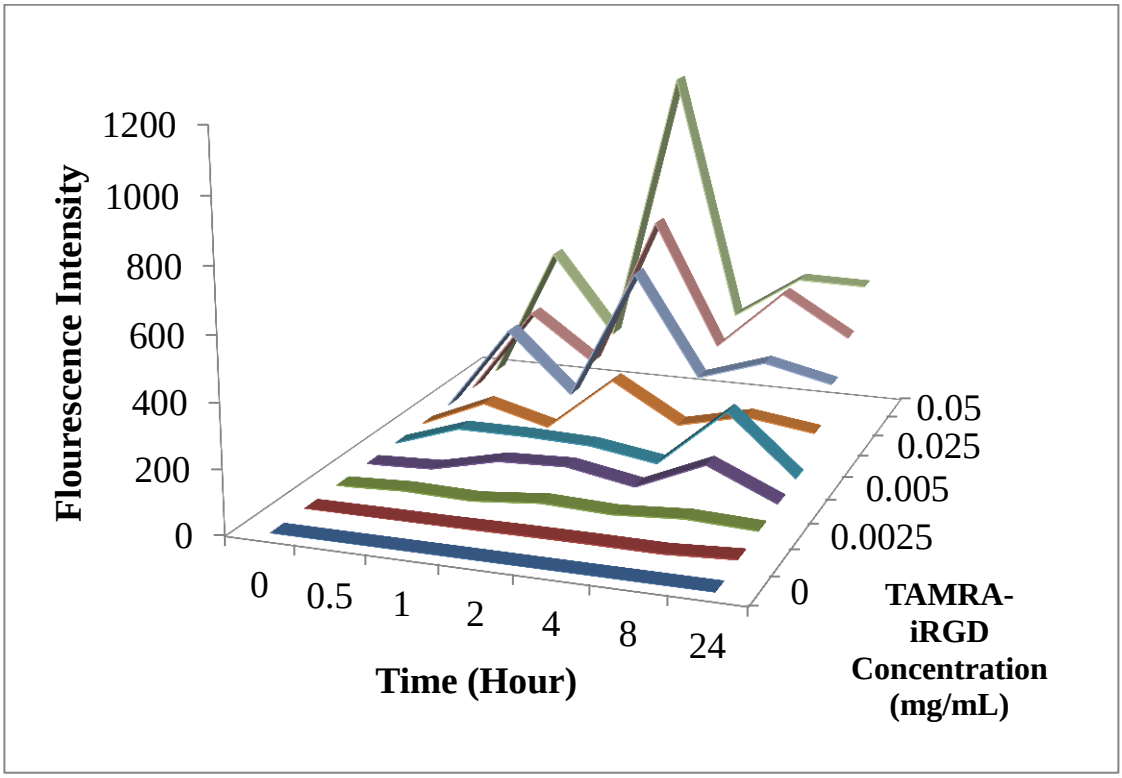

Figure 18: Results indicating the iRGD affinity to A549 lung adenocarcinoma cells. A549 cells were exposed to different concentrations of TAMRA-iRGD for up to 24 hours. The fluorescence intensity of the TAMRA-iRGD was then evaluated.

CHAPTER 4

CONCLUSIONS AND FUTURE WORK

4.1 Conclusions

Two kinds of drug-loaded nanoparticles were successfully synthesized using the polymer acetalated dextran in this study. These systems were comprised of 0.1% paclitaxel (PTX) and 10% imatinib-loaded nanoparticles. Overall, their physical and chemical characteristics have been evaluated. The developed systems exhibited favorable size (diameter), polydispersity in relation to size, and zeta potential to allow for their use in the systemic delivery of anticancer therapeutics. Both the encapsulation efficiency and drug loading were also favorable for the application of these nanoparticles for potential the treatment of lung cancer.

In vitro cell studies showed that drug-loaded nanoparticles increases the efficacy of chemotherapeutic drugs (in particular paclitaxel) for A549 lung carcinoma cells. It is possible that chemotherapeutic drug-loaded Ac-Dex nanoparticles could be applied *in vivo* to treat non-small cell lung cancer while reducing the toxic side effects of the free drug normally delivered systemically.

For this application, drug-loaded Ac-Dex nanoparticles could potentially be actively targeted to non-small cell lung cancer tumors and vasculature and then penetrate into the tumors cells with the help of tumor-penetrating peptide, iRGD. This intracellular environment would then trigger the intracellular burst release of the drug payload due to the acid-sensitivity of the Ac-Dex polymer with minimal drug released

in extracellular pH-neutral environments. The results of the described study indicate that iRGD can be successfully conjugated to Ac-Dex nanoparticles and that iRGD also shows affinity for A549 cells that are known to overexpress integrins that allow active targeting of the nanoparticle systems. Overall, these drug-loaded nanoparticles may have the ability to treat non-small lung cancer in addition to numerous other types of cancer.

4.2 Future Work

The work described in this thesis is hopefully just the beginning regarding the investigation of tandem delivery of agents using nanoparticles system for the treatment of non-small cell lung cancer. Future work to build upon this project may include, but is not limited to:

- Optimization of nanoparticles size and encapsulation efficiency to achieve a better effect during *in vitro* studies.
- Investigation of the methods of loading two drugs into one nanoparticle system to reduce side effects and allow for dual delivery.
- Optimizing and evaluating the conjugation of iRGD onto blank and drug-loaded nanoparticle systems.
- Investigation into the ability of iRGD-conjugated nanoparticles to increase the efficacy of non-iRGD nanoparticles against A549 cells on both 2D monolayer and 3D spheroid cultures.

- Evaluating the ability of iRGD-conjugated nanoparticles to penetrate 3D multicellular spheroids.
- Evaluating the systemic efficacy of iRGD-conjugated Ac-Dex nanoparticles *in vivo* in both non-small cell lung cancer cells and tissues.
- Incorporation of iRGD-conjugated, drug-loaded nanoparticles with radiation treatment to increase their therapeutic effect.

APPENDIX A

CALIBRATION CURVES

As described in Chapter 2 (Materials and Methods), calibration curves for paclitaxel (PTX) and imatinib mesylate (IM) were generating using ultra performance liquid chromatography (UPLC). As seen in **Figure A1**, a plot of the peak area due to the detection of PTX compared to its concentration was generated. This figure shows a lower detection limit of 10 μg/ml and upper detection limit of 80 μg/ml in the mobile phase for PTX. The R-squared value of 0.9999 shows very good fit for the described data. A plot of peak area due to the detection of IM compared to its concentration can be found in **Figure A2.** This figure shows a lower detection limit of 10 μg/ml and upper detection limit of 100 μg/ml for imatinib mesylate in mobile phase with a favorable R-squared value of 0.9944.

TAMRA-iRGD calibration curves were generated using fluorescence detection of a plate reader as described in Chapter 2 (Materials and Methods) as seen in **Figure A3**. For this detection, the lower limit was 0.0005 μg/ml and the upper limit was 0.05 μg/ml with a favorable R-squared value of 0.9. Finally an iRGD-fluorescamine calibration curve was generated using fluorescence microscopy. As seen in **Figure A4**, the lower limit was 0.1 mg/ml iRGD and the upper limit was 0.5 mg/ml with a favorable R-squared value of 0.9716.

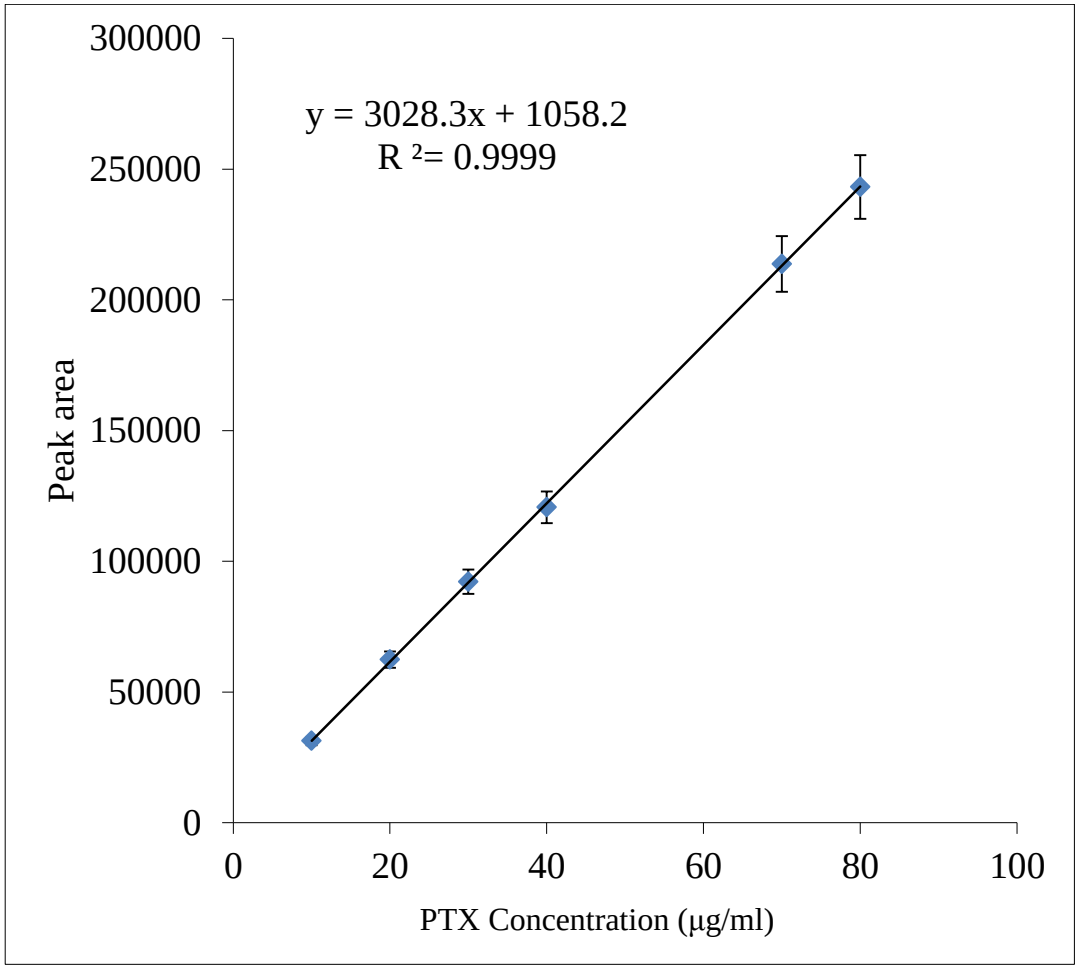

Figure 19: Calibration curve for paclitaxel (PTX) generated using ultra performance liquid chromatography (UPLC).

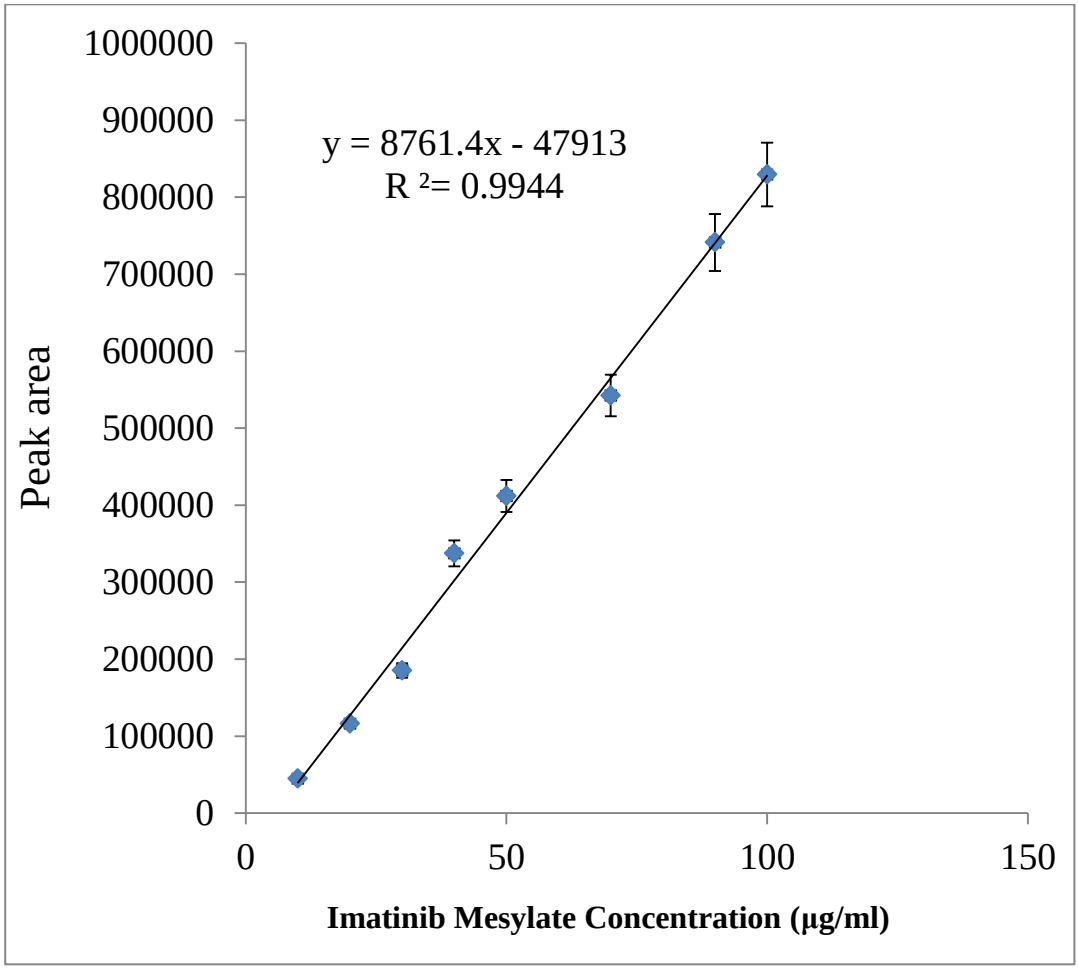

Figure 20: Calibration curve for imatinib mesylate (IM) generated using ultra performance liquid chromatography (UPLC).

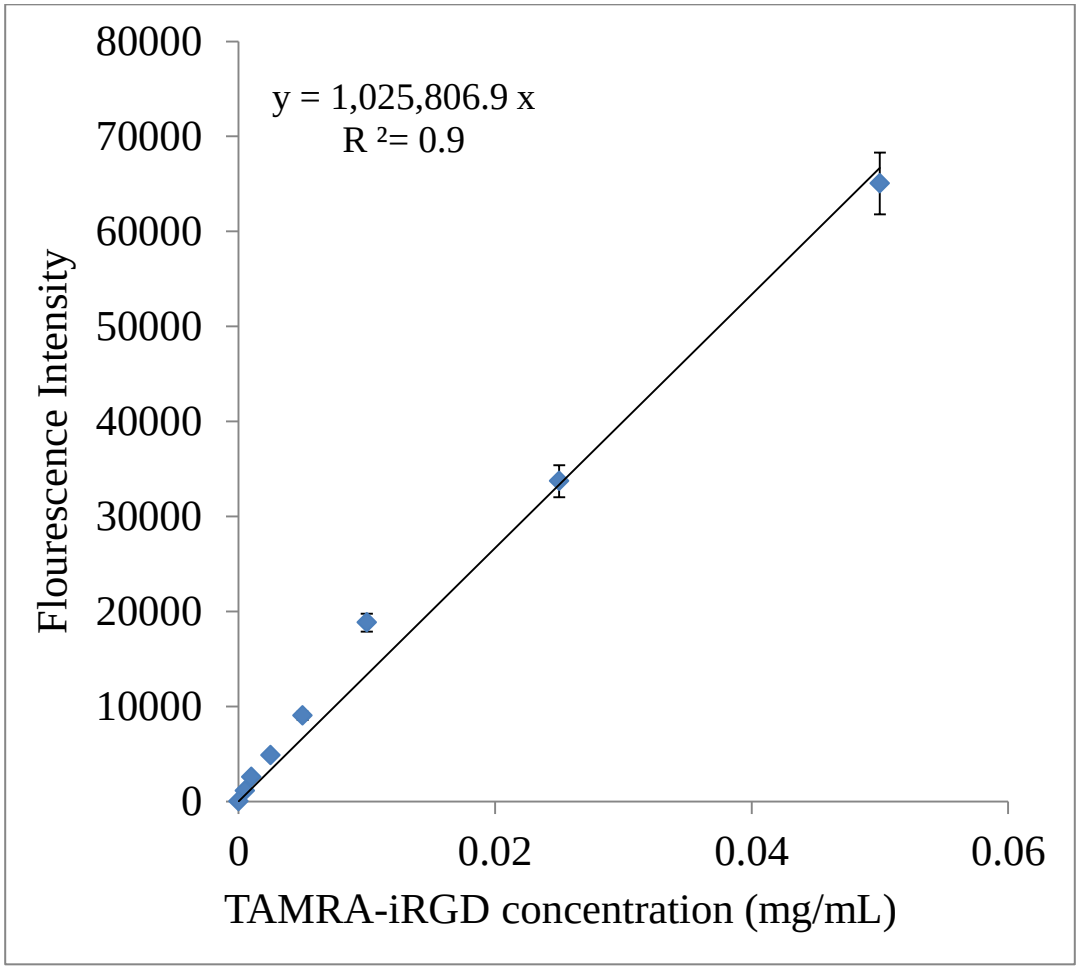

Figure 21: Calibration curve for TAMRA-iRGD as generated using fluorescence spectroscopy (plate reader).

APPENDIX B

^{1}H-NMR CALCULATIONS FOR AC-DEX

The cyclic acetal coverage (CAC) of Ac-Dex was determined using ^{1}H-NMR as described in Section 2.2 (Synthesis and Characterization of Acetalated Dextran (Ac-Dex)). Using the software available on the equipment, the areas of characteristic peaks of several compounds were calculated. These included the peak areas for the hydrogen rings present in dextran (3.4 to 4.0 ppm, three peaks total), methanol (3.36 ppm), and acetone (2.08 ppm). First, a normalization factor was calculated for the dextran peaks:

$$Normalization\ Factor\ (NF) = \frac{Average\ of\ Dextran\ Peaks}{2}$$

where 2 is the number of protons available on each molecule. Next the amount of methanol (MeOH) and acetone (Ace) present in the samples was calculated using the following equations:

$$MeOH = \frac{Methanol\ Peak\ Area}{3 * NF}$$

$$Ace = \frac{Acetone\ Peak\ Area}{6 * NF}$$

where NF is the normalization factor. NF was multiplied by 3 for the methanol samples and by 6 for the acetone samples owing to the number of hydrogen molecules present in these compounds. Finally, the cyclic acetal coverage (CAC) was calculated to be:

$$CAC = (Ace - MeOH)\ x\ 100\%$$

The extent of -OH hydrolysis was also calculated via ^{1}H-NMR analysis:

$$Cyclic\ acetal\ per\ glucose\ = Ace - MeOH$$

$$Acyclic\ acetal\ per\ glucose\ = MeOH$$

Two of the three and one of three hydroxyls on each glucose repeat unit can be used to form a single cyclic acetal and acyclic acetal, respectively. The number of -OH groups converted per glucose (-OH Conv) was calculated as:

$$-OH\ Conv = MeOH + 2(Ace - MeOH)$$

The percent acetalation ratio was then calculated as:

$$\%\ Acetalation = \frac{-OH\ Conv}{3}\ x\ 100\%$$

APPENDIX C

CALCULATIONS FOR DETERMINING IRGD COVERAGE

The number of iRGD molecules present on the surface of the Ac-Dex nanoparticles was determined using the fluorescamine assay. Fluorescamine reacts with primary amines on iRGD to allow for quantification of the amount of iRGD present in solution. As seen in **Figure 22**, there is a linear relationship between the fluorescence intensity of fluorescamine and the concentration of iRGD in PBS. Therefore, the amount of iRGD present on nanoparticles and the iRGD coverage per nanoparticle can be calculated from the following calculations. From the fluorescamine assay, the mass of iRGD present in the sample (m_{iRGD}) was 0.623 mg. From this value, the molecules of iRGD per sample was calculated as:

$$Molecules\ of\ iRGD = \frac{m_{iRGD} \cdot N_A}{MW}$$

where MW is the molecular weight of iRGD (1569.71 g/moles) and N_A is Avogadro's number (6.02214 x 10^{23} molecules/mole). The molecules of iRGD in 1 ml of solution was determined to be 3.969 x 10^{16} molecules. The number of nanoparticles present in each sample was determined from the nanoparticle volume, density, and mass per sample. The mass of an individual nanoparticle is calculated as:

$$Mass\ of\ single\ NP\ (m_n) = V\rho$$

where V is the volume of a 255 nm nanoparticle (1.413 x 10^7 nm^3) and ρ is the density of the nanoparticle (1 g/cm^3), which is the density of most polymers. This gives a mass of a single nanoparticle to be 1.413 x 10^{-11} mg. The number of nanoparticles in a sample was then calculated from the total mass of nanoparticle (m_T = 5 mg) and mass of a single nanoparticle:

$$\#\ of\ Nanoparticles = \frac{m_T}{m_n}$$

where the total number of nanoparticles per sample was 7.065 x 10^{11}. The number of iRGD present on each nanoparticle was then calculated from the number of nanoparticle (m_n) and number of iRGD molecules:

$$iRGD\ molecules\ per\ nanoparticle = \frac{Molecules\ of\ iRGD}{Number\ of\ Nanoparticles}$$

The number of iRGD molecules per nanoparticles was calculated to be 5.618 x 10^4. The iRGD coverage was then calculated form the number of iRGD molecules per nanoparticle and surface area of a single nanoparticle (A = 1.96 x 10^5 nm^2):

$$iRGD\ Coverage = \frac{iRGD\ molecules\ per\ nanoparticle}{A}$$

It was determined that there are 0.287 molecules of iRGD per nm^2 of particle area.

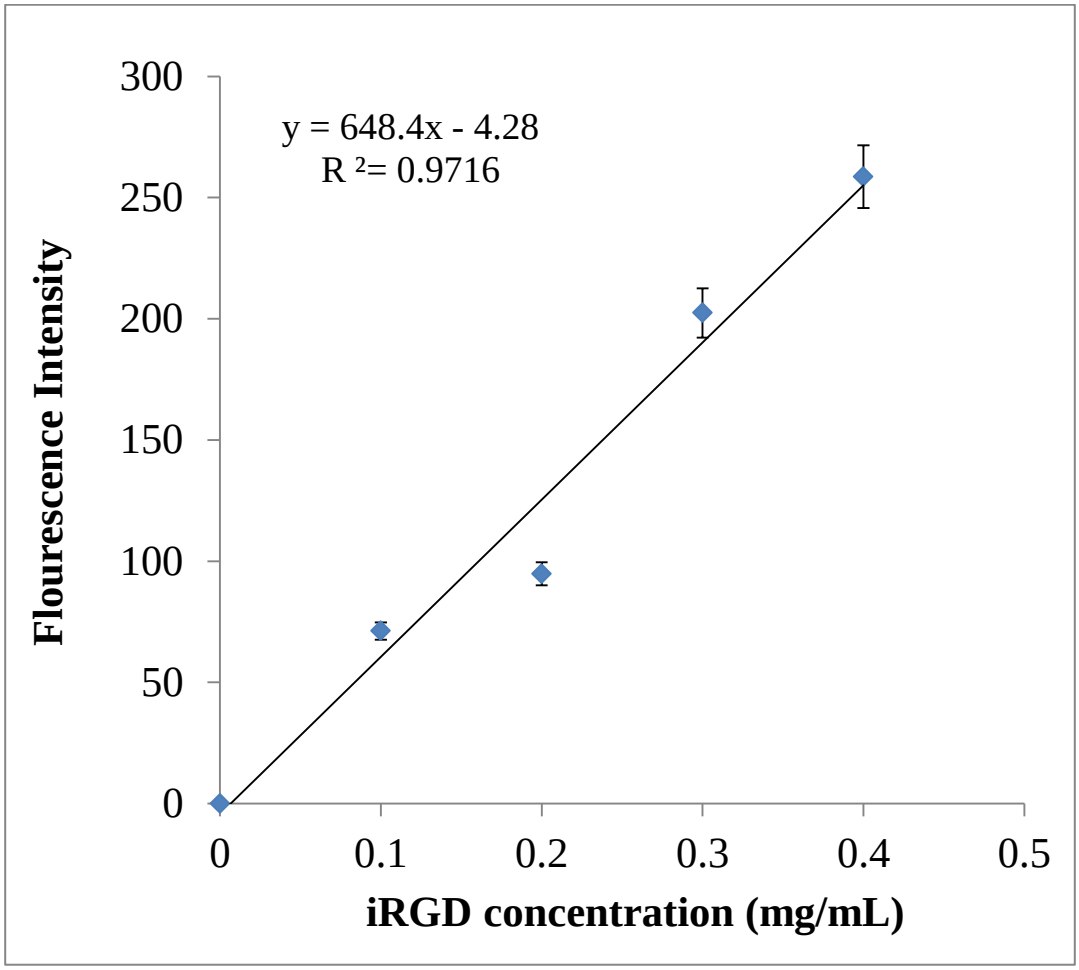

Figure 22: iRGD calibration curve as generated using fluorescence spectroscopy (plate reader).

BIBLIOGRAPHY

Abhilash, M. (2010). "Potential applications of Nanoparticles." International Journal of Pharma & Bio Sciences **1**(1).

Abramoff, M. D., P. J. Magalhaes and S. J. Ram (2004). "Image Processing with ImageJ." Biophotonics International **11**(7): 36-42.

Acharya, S. and S. K. Sahoo (2011). "Sustained targeting of Bcr–Abl+ leukemia cells by synergistic action of dual drug loaded nanoparticles and its implication for leukemia therapy." Biomaterials **32**(24): 5643-5662.

Aryal, S., C. M. J. Hu and L. Zhang (2010). "Combinatorial Drug Conjugation Enables Nanoparticle Dual‐Drug Delivery." Small **6**(13): 1442-1448.

Bachelder, E. M., T. T. Beaudette, K. E. Broaders, J. Dashe and J. M. Fréchet (2008). "Acetal-derivatized dextran: an acid-responsive biodegradable material for therapeutic applications." Journal of the American Chemical Society **130**(32): 10494-10495.

Bachelder, E. M., T. T. Beaudette, K. E. Broaders, J. Dashe and J. M. J. Fréchet (2008). "Acetal-Derivatized Dextran: An Acid-Responsive Biodegradable Material for Therapeutic Applications." Journal of the American Chemical Society **130**(32): 10494-10495.

Bachelder, E. M., T. T. Beaudette, K. E. Broaders, S. E. Paramonov, J. Dashe and J. M. Fréchet (2008). "Acid-degradable polyurethane particles for protein-based vaccines: biological evaluation and in vitro analysis of particle degradation products." Molecular pharmaceutics **5**(5): 876-884.

Barichello, J. M., M. Morishita, K. Takayama and T. Nagai (1999). "Encapsulation of hydrophilic and lipophilic drugs in PLGA nanoparticles by the nanoprecipitation method." Drug development and industrial pharmacy **25**(4): 471-476.

Beaudette, T. T., J. A. Cohen, E. M. Bachelder, K. E. Broaders, J. L. Cohen, E. G. Engleman and J. M. J. Frechet (2009). "Chemoselective Ligation in the Functionalization of Polysaccharide-Based Particles." Journal of the American Chemical Society **131**(30): 10360-+.

Braunecker, W. A. and K. Matyjaszewski (2007). "Controlled/living radical polymerization: features, developments, and perspectives." Progress in Polymer Science **32**(1): 93-146.

Broaders, K. E., J. A. Cohen, T. T. Beaudette, E. M. Bachelder and J. M. Fréchet (2009). "Acetalated dextran is a chemically and biologically tunable material for particulate immunotherapy." Proceedings of the National Academy of Sciences **106**(14): 5497-5502.

Broaders, K. E., J. A. Cohen, T. T. Beaudette, E. M. Bachelder and J. M. J. Frechet (2009). "Acetalated dextran is a chemically and biologically tunable material for

particulate immunotherapy." Proceedings of the National Academy of Sciences of the United States of America **106**(14): 5497-5502.

Carvalho, T. C., S. R. Carvalho and J. T. McConville (2011). "Formulations for pulmonary administration of anticancer agents to treat lung malignancies." Journal of aerosol medicine and pulmonary drug delivery **24**(2): 61-80.

Charcosset, C., A. A. El-Harati and H. Fessi (2006). "A membrane contactor for the preparation of solid lipid nanoparticles." Desalination **200**(1): 570-571.

Chetty, C., S. S. Lakka, P. Bhoopathi and J. S. Rao (2010). "MMP-2 alters VEGF expression via alpha v beta 3 integrin-mediated PI2K/AKT signaling in A549 lung cancer cells." International Journal of Cancer **127**: 1081-1095.

Cortese, B., S. D'Amone, G. Gigli and I. E. Palamà (2014). "Sustained anti BCR-ABL activity with pH responsive Imatinib Mesylate loaded PCL nanoparticles in CML cells." Med. Chem. Commun.

Danhier, F., N. Lecouturier, B. Vroman, C. Jérôme, J. Marchand-Brynaert, O. Feron and V. Préat (2009). "Paclitaxel-loaded PEGylated PLGA-based nanoparticles: in vitro and in vivo evaluation." Journal of Controlled Release **133**(1): 11-17.

Desgrosellier, J. S. and D. A. Cheresh (2010). "Integrins in cancer: biological implications and therapeutic opportunities." Nature Reviews Cancer **10**(1): 9-22.

Fessi, H., F. Puisieux, J. P. Devissaguet, N. Ammoury and S. Benita (1989). "Nanocapsule formation by interfacial polymer deposition following solvent displacement." International journal of pharmaceutics **55**(1): R1-R4.

Fife, T. H. and L. Jao (1965). "Substituent effects in acetal hydrolysis." The Journal of Organic Chemistry **30**(5): 1492-1495.

Galindo-Rodriguez, S., E. Allemann, H. Fessi and E. Doelker (2004). "Physicochemical parameters associated with nanoparticle formation in the salting-out, emulsification-diffusion, and nanoprecipitation methods." Pharmaceutical research **21**(8): 1428-1439.

Ganachaud, F. and J. L. Katz (2005). "Nanoparticles and Nanocapsules Created Using the Ouzo Effect: Spontaneous Emulsification as an Alternative to Ultrasonic and High ‐ Shear Devices." ChemPhysChem **6**(2): 209-216.

Gaudin, F. and N. Sintes-Zydowicz (2008). "Core–shell biocompatible polyurethane nanocapsules obtained by interfacial step polymerisation in miniemulsion." Colloids and Surfaces A: Physicochemical and Engineering Aspects **331**(1): 133-142.

Goodman, T. T., J. Chen, K. Matveev and S. H. Pun (2008). "Spatio ‐ temporal modeling of nanoparticle delivery to multicellular tumor spheroids." Biotechnology and bioengineering **101**(2): 388-399.

Goodman, T. T., P. L. Olive and S. H. Pun (2007). "Increased nanoparticle penetration in collagenase-treated multicellular spheroids." International journal of nanomedicine **2**(2): 265.

Green, M., G. Manikhas, S. Orlov, B. Afanasyev, A. Makhson, P. Bhar and M. Hawkins (2006). "Abraxane®, a novel Cremophor®-free, albumin-bound particle form of paclitaxel for the treatment of advanced non-small-cell lung cancer." Annals of Oncology **17**(8): 1263-1268.

Honary, S. and F. Zahir (2013). "Effect of Zeta Potential on the Properties of Nano-Drug Delivery Systems - A Review (Part 1)." Tropical Journal of Pharmaceutical Research **12**(2): 255-264.

Honary, S. and F. Zahir (2013). "Effect of Zeta Potential on the Properties of Nano-Drug Delivery Systems - A Review (Part 2)." Tropical Journal of Pharmaceutical Research **12**(2): 265-273.

Ingram, M., G. Techy, B. Ward, S. Imam, R. Atkinson, H. Ho and C. Taylor (2010). "Tissue engineered tumor models." Biotechnic & Histochemistry **85**(4): 213-229.

Jain, R. K. (1990). "Vascular and interstitial barriers to delivery of therapeutic agents in tumors." Cancer and Metastasis Reviews **9**(3): 253-266.

Jain, R. K. and T. Stylianopoulos (2010). "Delivering nanomedicine to solid tumors." Nature reviews clinical oncology **7**(11): 653-664.

Jeon, H.-J., Y.-I. Jeong, M.-K. Jang, Y.-H. Park and J.-W. Nah (2000). "Effect of solvent on the preparation of surfactant-free poly (DL-lactide-co-glycolide) nanoparticles and norfloxacin release characteristics." International journal of pharmaceutics **207**(1): 99-108.

Jeong, Y. I., C. S. Cho, S. H. Kim, K. S. Ko, S. I. Kim, Y. H. Shim and J. W. Nah (2001). "Preparation of poly (DL‐lactide‐co‐glycolide) nanoparticles without surfactant." Journal of applied polymer science **80**(12): 2228-2236.

Jinhyang, C., P. Jaesook and J. Dong-Hoon (2012). "Enhancement of Radiotherapeutic Efficacy by Paclitaxel-Loaded ph-Sensitive Block Copolymer Micelles."

Kanthamneni, N., S. Sharma, S. A. Meenach, B. Billet, J. C. Zhao, E. M. Bachelder and K. M. Ainslie (2012). "Enhanced stability of horseradish peroxidase encapsulated in acetalated dextran microparticles stored outside cold chain conditions." International Journal of Pharmaceutics **431**(1-2): 101-110.

Karmali, P. P., V. R. Kotamraju, M. Kastantin, M. Black, D. Missirlis, M. Tirrell and E. Ruoslahti (2009). "Targeting of albumin-embedded paclitaxel nanoparticles to tumors." Nanomedicine **5**(1): 73-82.

Kauffman, K. J., N. Kanthamneni, S. A. Meenach, B. C. Pearson, E. M. Bachelder and K. M. Ainslie (2011). "Optimization of Rapamycin-Loaded Acetalated Dextran Microparticles for Immunosuppression." International Journal of Pharmaceutics **422**: 356-363.

Kawashima, Y. (2001). "Nanoparticulate systems for improved drug delivery." Advanced Drug Delivery Reviews **47**(1): 1-2.

Kayser, O., A. Lemke and N. Hernandez-Trejo (2005). "The impact of nanobiotechnology on the development of new drug delivery systems." Current pharmaceutical biotechnology **6**(1): 3-5.

Kelly, K., J. Crowley, P. A. Bunn, C. A. Presant, P. K. Grevstad, C. M. Moinpour, S. D. Ramsey, A. J. Wozniak, G. R. Weiss and D. F. Moore (2001). "Randomized phase III trial of paclitaxel plus carboplatin versus vinorelbine plus cisplatin in the treatment of patients with advanced non–small-cell lung cancer: a Southwest Oncology Group trial." Journal of Clinical Oncology **19**(13): 3210-3218.

Kimura, S., K. Egashira, K. Nakano, E. Iwata, M. Miyagawa, H. Tsujimoto, K. Hara, Y. Kawashima, R. Tominaga and K. Sunagawa (2008). "Local delivery of imatinib mesylate (STI571)-incorporated nanoparticle ex vivo suppresses vein graft neointima formation." Circulation **118**(14 suppl 1): S65-S70.

Kochanski, J., R. R. WEIcHSELBAUM and E. E. VoKES (2012). "Everolimus exhibits efficacy as a radiosensitizer in a model of non-small cell lung cancer." Oncology reports **27**: 1625a1629.

Kostag, M., S. Köhler, T. Liebert and T. Heinze (2010). Pure cellulose nanoparticles from trimethylsilyl cellulose. Macromolecular symposia, Wiley Online Library.

Lambert, G., E. Fattal, H. Pinto-Alphandary, A. Gulik and P. Couvreur (2000). "Polyisobutylcyanoacrylate nanocapsules containing an aqueous core as a novel colloidal carrier for the delivery of oligonucleotides." Pharmaceutical research **17**(6): 707-714.

Landfester, K., A. Musyanovych and V. Mailänder (2010). "From polymeric particles to multifunctional nanocapsules for biomedical applications using the miniemulsion process." Journal of Polymer Science Part A: Polymer Chemistry **48**(3): 493-515.

Lin, R. Z. and H. Y. Chang (2008). "Recent advances in three‐dimensional multicellular spheroid culture for biomedical research." Biotechnology Journal **3**(9‐10): 1172-1184.

Marupudi, N. I., J. E. Han, K. W. Li, V. M. Renard, B. M. Tyler and H. Brem (2007). "Paclitaxel: a review of adverse toxicities and novel delivery strategies." Expert Opinion on Drug Safety **6**: 609-621.

Meenach, S. A., Y. J. Kim, K. J. Kauffman, N. Kanthamneni, E. M. Bachelder and K. M. Ainslie (2012). "Synthesis, Optimization, and Characterization of Camptothecin-Loaded Acetalated Dextran Porous Microparticles for Pulmonary Delivery." Molecular Pharmaceutics **9**(2): 290-298.

NCI, N. (2014). "SEER Training Modules." Lung Cancer, from http://training.seer.cancer.gov/lung/intro/types.html.

Niwa, T., H. Takeuchi, T. Hino, N. Kunou and Y. Kawashima (1993). "Preparations of biodegradable nanospheres of water-soluble and insoluble drugs with D, L-lactide/glycolide copolymer by a novel spontaneous emulsification solvent diffusion method, and the drug release behavior." Journal of controlled release **25**(1): 89-98.

Odrljin, T., C. G. Haidaris, N. B. Lerner and P. J. Simpson-Haidaris (2001). "Integrin alpha v beta 3-mediated endocytosis of immobilized fibrinogen by A549 lung alveolar epithelial cells." American Journal of Respiratory Cell and Molecular Biology **24**: 12-21.

Pinto Reis, C., R. J. Neufeld, A. J. Ribeiro and F. Veiga (2006). "Nanoencapsulation I. Methods for preparation of drug-loaded polymeric nanoparticles." Nanomedicine: Nanotechnology, Biology and Medicine **2**(1): 8-21.

Rao, J. P. and K. E. Geckeler (2011). "Polymer nanoparticles: preparation techniques and size-control parameters." Progress in Polymer Science **36**(7): 887-913.

Ruoslahti, E., S. N. Bhatia and M. J. Sailor (2010). "Targeting of drugs and nanoparticles to tumors." JCB: Review **188**(6): 759-768.

Sajja, H. K., M. P. East, H. Mao, A. Y. Wang, S. Nie and L. Yang (2009). "Development of multifunctional nanoparticles for targeted drug delivery and non-invasive imaging of therapeutic effect." Current drug discovery technologies **6**(1): 43.

Schiller, J. H., D. Harrington, C. P. Belani, C. Langer, A. Sandler, J. Krook, J. Zhu and D. H. Johnson (2002). "Comparison of four chemotherapy regimens for advanced non–small-cell lung cancer." New England Journal of Medicine **346**(2): 92-98.

Schroedl, C. and R. Kalhan (2012). "Incidence, treatment options, and outcomes of lung cancer in patients with chronic obstructive pulmonary disease." Current opinion in pulmonary medicine **18**(2): 131-137.

Simberg, D., T. Duza, J. H. Park, M. Essler, J. Pilch, L. Zhang, A. M. Derfus, M. Yang, R. M. Hoffman, S. N. Bhatia, M. J. Sailor and E. Ruoslahti (2007). "Biomimetic amplification of nanoparticle homing to tumors." Proceedings of the National Academy of Sciences **104**(3): 932-936.

Sinha, R., G. J. Kim, S. Nie and D. M. Shin (2006). "Nanotechnology in cancer therapeutics: bioconjugated nanoparticles for drug delivery." Molecular cancer therapeutics **5**(8): 1909-1917.

Sneed, P. K., P. R. Stauffer, M. W. McDermott, C. J. Diederich, K. R. Lamborn, M. D. Prados, S. Chang, K. A. Weaver, L. Spry and M. K. Malec (1998). "Survival benefit of hyperthermia in a prospective randomized trial of brachytherapy boost±hyperthermia for glioblastoma multiforme." International Journal of Radiation Oncology* Biology* Physics **40**(2): 287-295.

Sugahara, K. N., T. Teesalu, P. P. Karmali, V. R. Kotamraju, L. Agemy, O. M. Girard, D. Hanahan, R. F. Mattrey and E. Ruoslahti (2009). "Tissue-penetrating delivery of compounds and nanoparticles into tumors." Cancer cell **16**(6): 510-520.

Sugahara, K. N., T. Teesalu, P. P. Karmali, V. R. Kotamraju, L. Agemy, O. M. Girard, D. Hanahan, R. F. Mattrey and E. Ruoslahti (2009). "Tissue-penetrating delivery of compounds and nanoparticles into tumors." Cancer Cell **16**: 510-520.

Sugahara, K. N., T. Teesalu, P. P. Karmali, V. R. Kotamraju, L. Agemy, D. R. Greenwald and E. Ruoslahti (2010). "Coadministration of a tumor-penetrating peptide enhances the efficacy of cancer drugs." science **328**(5981): 1031-1035.

Sundaram, S., R. Trivedi, C. Durairaj, R. Ramesh, B. K. Ambati and U. B. Kompella (2009). "Targeted drug and gene delivery systems for lung cancer therapy." Clinical Cancer Research **15**(23): 7299-7308.

Timeus, F., N. Crescenzio, A. Doria, L. Foglia, S. Pagliano, E. Ricotti, F. Fagioli, P. A. Tovo, L. C. H. Montezemolo and L. Cordero (2012). "In vitro anti-neuroblastoma activity of saquinavir and its association with imatinib." Oncology reports **27**(3): 734.

Vermeulen, K., D. R. Van Bockstaele and Z. N. Berneman (2003). "The cell cycle: A review of regulation deregulation and therapeutic agents in cancer." Cell Proliferation **36**: 131-149.

Waite, C. L. and C. M. Roth (2009). "PAMAM-RGD conjugates enhance siRNA delivery through a multicellular spheroid model of malignant glioma." Bioconjugate chemistry **20**(10): 1908-1916.

Wisnivesky, J. P., M. Bonomi, C. Henschke, M. Iannuzzi and T. McGinn (2005). "Radiation therapy for the treatment of unresected stage I-II non-small cell lung cancer." CHEST Journal **128**(3): 1461-1467.

Wu, M., E. Dellacherie, A. Durand and E. Marie (2009). "Poly (< i> n</i>-butyl cyanoacrylate) nanoparticles via miniemulsion polymerization. 2. PEG-based surfactants." Colloids and Surfaces B: Biointerfaces **69**(1): 147-151.

York, P. (1999). "Strategies for particle design using supercritical fluid technologies." Pharmaceutical science & technology today **2**(11): 430-440.

Young, R. P., R. J. Hopkins, T. Christmas, P. N. Black, P. Metcalf and G. D. Gamble (2009). "COPD prevalence is increased in lung cancer, independent of age, sex and smoking history." European Respiratory Journal **34**(2): 380-386.

Zhang, P., W. Y. Gao, S. Turner and B. S. Ducatman (2003). "Gleevec (STI-571) inhibits lung cancer cell growth (A549) and potentiates the cisplatin effect in vitro." Molecular cancer **2**(1): 1.

Zhang, X., H. Yang, K. Gu, J. Chen, M. Rui and G.-L. Jiang (2011). "In vitro and in vivo study of a nanoliposomal cisplatin as a radiosensitizer." Int J Nanomedicine **6**: 437-444.

Zhao, Y., W. Jiang, B. Li, Q. Yao, J. Dong, Y. Cen, X. Pan, J. Li, J. Zheng and X. Pang (2011). "Artesunate enhances radiosensitivity of human non-small cell lung cancer A549 cells via increasing NO production to induce cell cycle arrest at G< sub> 2</sub>/M phase." International immunopharmacology **11**(12): 2039-2046.